Landscape of Exhausted Virus-Specific CD8 T Cells in Chronic LCMV Infection

Author(s):
Sandu, Ioana; Cerletti, Dario; Oetiker, Nathalie; Borsa, Mariana; Wagen, Franziska; Spadafora, Ilaria; Welten, Suzanne P.M.; Stolz, Ugne; Oxenius, Annette; Claassen, Manfred

Publication date:
2020

Permanent link:
https://doi.org/10.3929/ethz-b-000438593

Originally published in:
Cell Reports 32(8), https://doi.org/10.1016/j.celrep.2020.108078

Cell Reports

Resource

Landscape of Exhausted Virus-Specific CD8 T Cells in Chronic LCMV Infection

Graphical Abstract

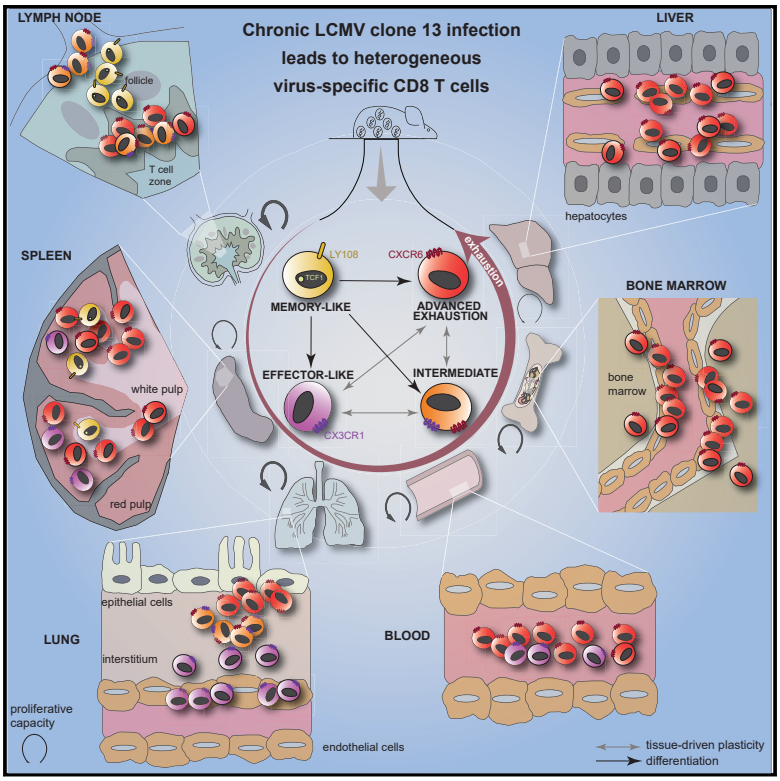

Highlights

- scRNA-seq analysis of exhausted cells reveals tissue-associated heterogeneity
- Exhausted P14 cells can be grouped into five plastic functional phenotypes
- Effector-like CX3CR1^{hi} cells are close to the circulation
- Cells in advanced state of exhaustion (CX3CR6^{hi}CX3CR1^{-}) are found in the tissues

Authors

Ioana Sandu, Dario Cerletti, Nathalie Oetiker, ..., Ugne Stolz, Annette Oxenius, Manfred Claassen

Correspondence

aoxenius@micro.biol.ethz.ch (A.O.), claassen@imsb.biol.ethz.ch (M.C.)

In Brief

Sandu et al. compare the transcriptional profile of exhausted virus-specific CD8 T cells isolated from six tissues of mice chronically infected with LCMV. They reveal exhausted cells are heterogeneous, adopt organ-specific signatures, and can be divided into five main functional subpopulations: advanced exhaustion, effector-like, intermediate, proliferating, and memory-like.

Sandu et al., 2020, Cell Reports *32*, 108078
August 25, 2020
https://doi.org/10.1016/j.celrep.2020.108078

CellPress

Cell Reports

CellPress
OPEN ACCESS

Resource

Landscape of Exhausted Virus-Specific CD8 T Cells in Chronic LCMV Infection

Ioana Sandu,[1,2,3] Dario Cerletti,[1,2,3] Nathalie Oetiker,[1] Mariana Borsa,[1] Franziska Wagen,[1] Ilaria Spadafora,[1] Suzanne P.M. Welten,[1] Ugne Stolz,[1] Annette Oxenius,[1,5,6,*] and Manfred Claassen[2,3,4,5,*]

[1]Institute of Microbiology, ETH Zürich, Vladimir-Prelog-Weg 4, 8093 Zürich, Switzerland
[2]Institute of Molecular Systems Biology, ETH Zürich, Otto-Stern-Weg 3, 8093 Zürich, Switzerland
[3]Swiss Institute of Bioinformatics, University of Lausanne, Quartier Sorge–Batiment Amphipole, 1015 Lausanne, Switzerland
[4]Present address: Internal Medicine I, University Hospital Tübingen, Faculty of Medicine, University of Tübingen, Otfried-Müller-Straße 10, 72076 Tübingen, Germany
[5]These authors contributed equally
[6]Lead Contact
*Correspondence: aoxenius@micro.biol.ethz.ch (A.O.), claassen@imsb.biol.ethz.ch (M.C.)
https://doi.org/10.1016/j.celrep.2020.108078

SUMMARY

A hallmark of chronic infections is the presence of exhausted CD8 T cells, characterized by a distinct transcriptional program compared with functional effector or memory cells, co-expression of multiple inhibitory receptors, and impaired effector function, mainly driven by recurrent T cell receptor engagement. In the context of chronic lymphocytic choriomeningitis virus (LCMV) infection in mice, most studies focused on studying splenic virus-specific CD8 T cells. Here, we provide a detailed characterization of exhausted CD8 T cells isolated from six different tissues during established LCMV infection, using single-cell RNA sequencing. Our data reveal that exhausted cells are heterogeneous, adopt organ-specific transcriptomic profiles, and can be divided into five main functional subpopulations: advanced exhaustion, effector-like, intermediate, proliferating, or memory-like. Adoptive transfer experiments showed that these phenotypes are plastic, suggesting that the tissue microenvironment has a major impact in shaping the phenotype and function of virus-specific CD8 T cells during chronic infection.

INTRODUCTION

Human immunodeficiency virus (HIV) and hepatitis virus in humans, or lymphocytic choriomeningitis virus (LCMV) in mice, are chronic infections where active viral replication is ongoing for weeks, months, or even years, leading to high systemic viral titers and antigen loads. In response to sustained exposure to cognate antigens, virus-specific CD8 T cells adopt a distinct transcriptional program (Wherry et al., 2007), epigenetic landscape (Sen et al., 2016), and phenotype (collectively termed exhaustion), compared with normal functional effector or memory CD8 T cells that develop following an acute infection (Wherry et al., 2003).

Exhausted CD8 T cells are characterized by sustained co-expression of inhibitory receptors, such as programmed cell death protein 1 (PD-1), LAG-3, 2B4, CD160, and CD39 (Blackburn et al., 2009; Richter et al., 2010; Gupta et al., 2015; Barber et al., 2006), impaired effector functions (loss of interleukin-2 [IL-2], interferon γ [IFN-γ], or tumor necrosis factor alpha [TNF-α] production), limited numbers, and altered requirements for population maintenance compared with classical memory cells (Wherry et al., 2003; Fuller et al., 2004). The transcription factor TOX (Khan et al., 2019; Seo et al., 2019; Yao et al., 2019) has been recently identified as the master regulator controlling the exhaustion program. Antigen, ongoing proliferation, and IL-21 are involved in overall maintenance of the exhausted virus-specific CD8 T cell pool (Fröhlich et al., 2009; Schmitz et al., 2013; Shin et al., 2007; Yi et al., 2009). Moreover, exhausted CD8 T cells are seemingly impaired in their ability to efficiently kill infected cells during chronic infection *in vivo*. However, when assessing their *in vitro* or *in vivo* killing capacity of naive target cells, cytotoxic potential is clearly observed (Agnellini et al., 2007; Garcia et al., 2015; Graw et al., 2011). Exhaustion is a gradual, continuous process that, among other factors, is triggered by persistent T cell receptor (TCR) stimulation, the degree of exhaustion depending on the TCR signaling strength, antigen abundance, and affinity (Utzschneider et al., 2016a; Mueller and Ahmed, 2009; Wherry et al., 2003). As a result, the pool of exhausted CD8 T cells is likely a heterogeneous population. Some studies suggested that the phenotype of exhausted virus-specific CD8 T cells depends on the tissue location (Wherry et al., 2003; Blackburn et al., 2010), but most transcriptional analyses are not informative about inter-tissue heterogeneity of LCMV-specific CD8 T cells during chronic infection because most studies focused on cells isolated from the spleen (Utzschneider et al., 2016b; Wherry et al., 2007; Scott-Browne et al., 2016). Two major subpopulations of exhausted CD8 T cells were described in secondary lymphoid tissues: a less exhausted

TCF1^{hi} T-bet^{hi} PD-1^{lo}, more functional population, termed memory-like, and a more terminally exhausted population TCF1^{neg} PD-1^{hi} EOMES^{hi} CD39^{hi} (Paley et al., 2013; Gupta et al., 2015; Utzschneider et al., 2016b). Additionally, single-cell RNA sequencing (scRNA-seq) of exhausted CD8 T cells isolated from the spleen revealed four distinct subsets: effector-like, proliferating, memory-like TCF1^{hi}, and terminally exhausted PD-1^{hi} CD39^{hi} (Miller et al., 2019; Hudson et al., 2019; Zander et al., 2019). This documents heterogeneity within the pool of virus-specific CD8 T cells during chronic infection present in secondary lymphoid organs; however, the extent of heterogeneity has not been resolved with respect to an unbiased selection of cell markers, as well as for other tissues than secondary lymphoid organs.

In this study, we evaluated the heterogeneity of single-cell transcriptomes of virus-specific CD8 T cells isolated from six different tissues (spleen, lymph nodes [LNs], bone marrow [BM], lung, liver, and blood) in mice with chronic LCMV infection. Overall, the population of virus-specific CD8 T cells could be classified into five functional phenotypes (memory-like, proliferating, effector-like, intermediate, and advanced state of exhaustion), based on distinct transcriptional profiles regarding T cell activation and inhibition, chemokine and IL receptors, and transcription factor expression. Cells with these functional phenotypes were represented at different frequencies in specific tissues, resulting in tissue-specific phenotype transcription profiles, most apparent in those tissues where the population of virus-specific CD8 T cells was predominantly composed of cells with a single functional phenotype.

RESULTS

Exhausted P14 Cells Exhibit Tissue-Specific Phenotypes

LCMV induces a systemic infection and infects a wide range of cells of both hematopoietic and non-hematopoietic origin, but not lymphocytes (Mims and Wainwright, 1968; Althage et al., 1992; Odermatt et al., 1991). Previous studies showed that viral loads vary among different tissues (Ciurea et al., 1999; Wherry et al., 2003). We therefore hypothesized that LCMV-specific CD8 T cells might adopt different phenotypes, depending on their tissue origin. We used LCMV $gp_{33–41}$ (peptide derived from LCMV glycoprotein containing amino acids 33 to 41)-specific TCR-transgenic CD8 T cells (P14 cells; Pircher et al., 1990) crossed to *Nr4a1*-GFP reporter mice (Moran et al., 2011) in adoptive transfer experiments, allowing isolation of this monoclonal population from various tissues during established chronic LCMV clone 13 infection. At 21 days into chronic infection, P14 cells were phenotyped by flow cytometry in six different tissues: spleen, LNs, BM, lung, liver, and blood. This phenotypic analysis was based on quantification of CD8, the activation markers NUR77 and CD44, and inhibitory receptors (PD-1, TIM-3, CD39). We evaluated phenotypic heterogeneity across the tissues with respect to these markers by means of a t-distributed stochastic neighbor embedding (t-SNE) projection (Figure S1). We observed that exhausted cells were heterogeneous within tissues and even more so between tissues, despite expressing the same TCR.

scRNA-Seq of P14 Cells Demonstrates Transcriptional Heterogeneity across Tissues

Having observed intra- and inter-tissue P14 heterogeneity based on a limited set of phenotypic markers, we sought to employ scRNA-seq to unbiasedly assess their heterogeneity during chronic LCMV infection in different tissues (Figure 1A). After pre-processing (see STAR Methods), cells were clustered using a graph-based clustering approach (Butler et al., 2018), and results were visualized with t-SNE (Maaten and Hinton, 2008; Figures 1B and 1C).

Overall, 14 distinct clusters with different transcriptional patterns (Table S1; Figure S2) were identified within P14 cells originating from various tissues (Figure 1D). Most clusters (8 out of 14) were composed of more than 80% cells isolated from one tissue only (Figure 1E). The number of analyzed P14 cells was comparable among tissues (Figure 1F), and the cluster size varied between 4,204 and 167 cells (Figure 1G). Although we cannot rule out that batch effects might impact the clustering, we believe that this is rather unlikely, because some clusters, such as 7, 10, and 11, were composed of cells from all samples (Figure 1E), suggesting that batch effects were not the main driver of variation. The most homogeneous samples were composed of cells isolated from BM and liver, with more than 70% of cells attributed to only one cluster, whereas cells isolated from blood, spleen, LN, and lung were more diverse, with at least two clusters making up for at least 10% of the cells (Figure 1D).

Factor Analysis Reveals Five Main Phenotypes with Distinct Transcriptional Signatures Regarding TCR Activation and Inhibition, Trafficking, and IL Receptors

Next, we assessed biologically relevant phenotypes of the above defined clusters. To this end, we employed factor decomposition analysis (Slalom; Buettner et al., 2017). This method identifies factors, i.e., predefined gene sets representing biological processes or functions that explain the observed variability in the scRNA-seq data. We considered gene sets defined by the immunological C7 collection from MSig (Godec et al., 2016) and found three factors of interest (Figures 2A–2C), which demarcated cells associated with proliferation, T cell memory, and T cell exhaustion (Figures 2D–2F). Gene set enrichment analysis (GSEA) performed on ranked genes correlating with expression of the factors confirmed significant enrichment of pathways related to proliferation, memory (Utzschneider et al., 2016b), exhaustion (Wherry et al., 2007), or effector signature (Doering et al., 2012; Figures 2G–2I). These three factors of CD8 T cell function suggest classification of P14 cells into five main functional phenotypes: proliferating (T_P), effector-like (T_E), memory-like (T_M), cells in an "advanced exhaustion" state (T_{Exh}), and intermediate between T_E and T_{Exh} (T_I). These main phenotypes were differentially represented in the tissues of interest (Figure 2J), with hallmark genes being differentially expressed (Figures 2K–2N).

The first factor denotes T_P cells, which exhibited higher expression of genes important in regulating the cell cycle and were found to have a very low frequency in all tissues (Figure 2J). GSEA performed on differentially expressed genes in cluster 7 (compared with all other cells) confirmed that cell-cycle and proliferation-related genes were overexpressed (Figure 2G;

CellPress
OPEN ACCESS

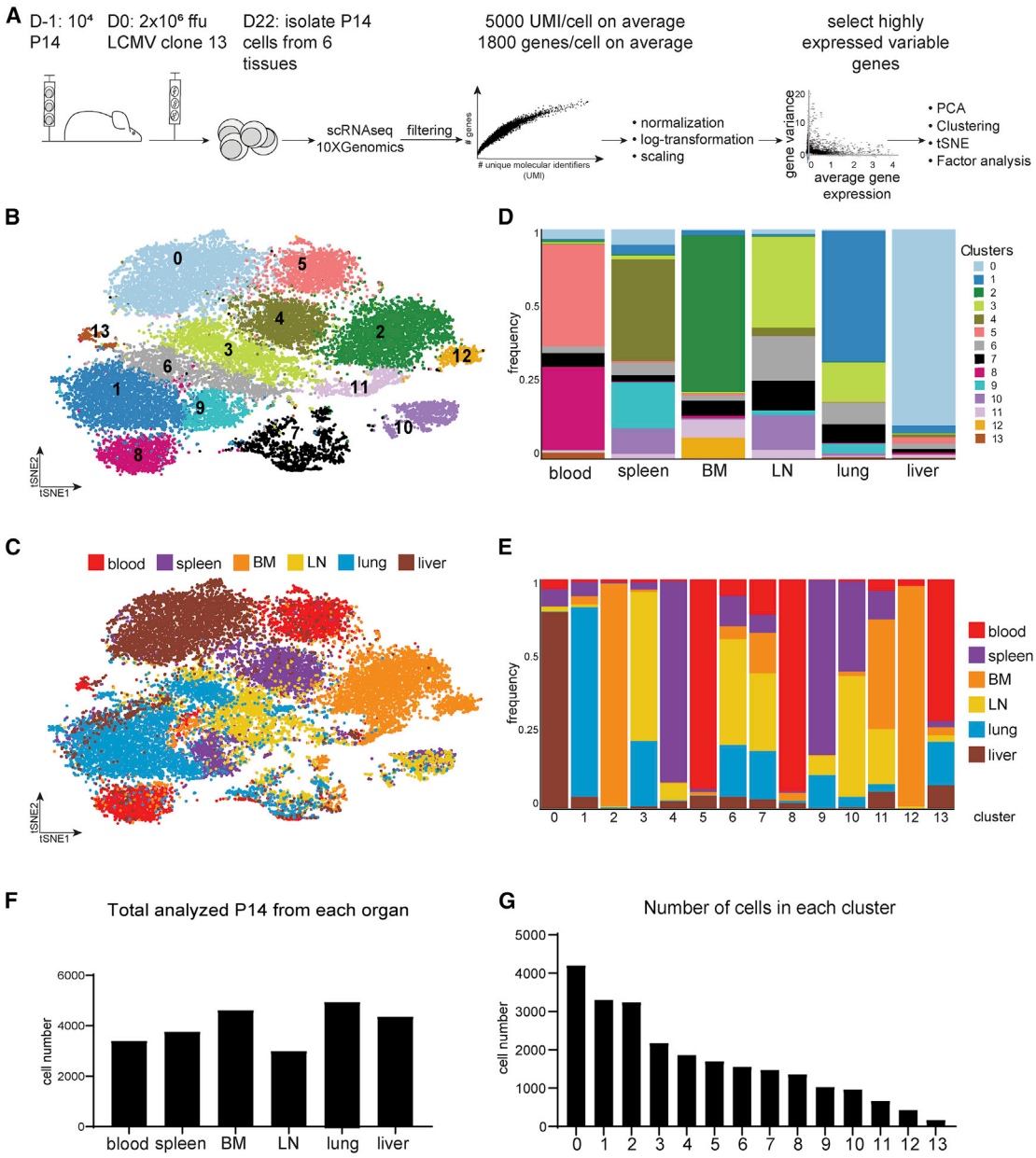

Figure 1. scRNA-seq Reveals P14 Heterogeneity

(A) P14 cells were isolated from tissues 21 days after LCMV infection. After pre-processing, highly expressed and variable genes were used to compute the first 20 principal components, which were used as input for t-SNE dimensionality reduction.

(B and C) t-SNE projection based on transcriptional profile. Each dot represents a cell and the color the cluster assignment (B) or the tissue of origin (C).

(D) Contribution of each cluster to the tissue samples.

(E) Contribution of each sample to clusters.

(F) P14 number analyzed by scRNA-seq per organ.

(G) Number of cells per cluster.

See also Table S1.

Figure S2). Among these, spindle assembly checkpoint *Mad2l1* (Li and Benezra, 1996), apoptosis inhibitor *Birc5* (Dohi et al., 2004), *Mki67* encoding Ki-67, cyclins and cyclin-dependent kinases (*Cdc8a*, *Cdc3*, *Cks1b*, *Cks2*), DNA replication licensing factors (*Mcm2*, *Mcm3*), DNA synthesis (*Lig1*), or elongation factors (*E2f1*) (Figures 2D and 2K) were expressed. Moreover, target genes of proliferation-related transcription factors, such as *Mybl2*, *Maz*, or *E2f1*, were also upregulated (Table S2). Interestingly, this cluster was composed of P14 cells isolated from all organs, suggesting that they are able to proliferate in the tissues.

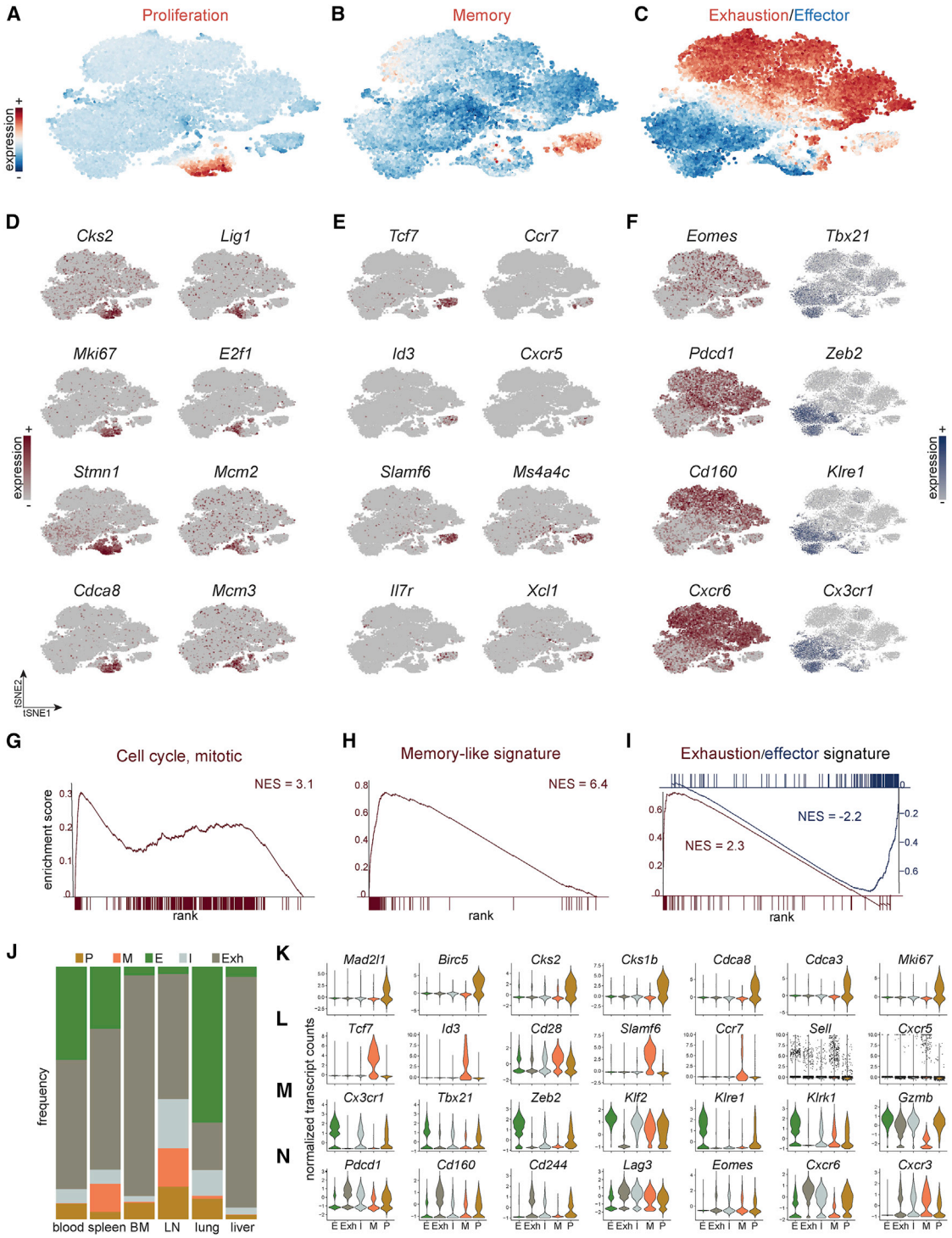

Figure 2. Functional Cluster Assignment

(A–F) Same projection (t-SNE) as in Figure 1. (A–C) Colors represent factors positively (red) or negatively (blue) associated with proliferation (A), memory (B), or exhaustion/effector (C) phenotypes. (D–F) Selected examples of genes associated with the phenotype depicted in (A)–(C). Color denotes transcripts positively (red) or negatively (blue) correlated with factors.

(G–I) GSEA performed on ranked genes correlating with identified factors in (A)–(C) were significantly enriched in the reference pathways depicted: cell cycle (G), memory-like signature of exhausted P14 TCF1^{+} (H), and exhaustion (red) or effector (blue) signature of P14 cells (I, in blue).

(legend continued on next page)

The second factor identified T_M cells (Figure 2B) and demarcated cluster 10. T_M cells were found only in the spleen and LNs (Figure 2J), as reported previously (Utzschneider et al., 2016b; Im et al., 2016). These cells expressed memory-associated transcription factors, such as *Tcf7* encoding TCF1 and *Id3*, and higher levels of *Cd28* (Figure 2L). They also expressed *Ccr7* and *Sell*, encoding CD62L (Figure 2L), which might explain why they are mainly found in secondary lymphoid organs (Berg et al., 1991; Gunn et al., 1998). Additionally, T_M cells expressed higher levels of *Slamf6* encoding Ly108 and *Cxcr5* (Figure 2L), which have been described as markers for a memory-like population with stem-like properties within virus-specific CD8 T cells in chronic LCMV infection, able to replenish the pool of exhausted CD8 T cells (Utzschneider et al., 2016b; Im et al., 2016) and being responsible for the proliferative burst observed following programmed death-ligand 1 (PD-L1) blockade (Utzschneider et al., 2016b; Im et al., 2016; Chamoto et al., 2017; Borsa et al., 2019). Genes highly correlated with the memory factor showed an enrichment in the $TCF1^+$ signature (Figure 2H). T_M cells expressed low levels of inhibitory receptors, effector molecules, and transcription factors associated with an effector program (*Tbx21*, *Id2*, *Zeb2*), but exhibited higher expression of *Tcf7* (Table S1), *Id3*, *Il7r*, *Sell*, and *Ccr7* (Figure 3). Moreover, target genes of *Tcf7* were also upregulated in cluster 10 (Table S2). T_M cells also expressed the chemokine receptor *Cxcr5* (Figure 2L), which might mediate migration of these cells into the white pulp (Utzschneider et al., 2018; Leong et al., 2016; Im et al., 2016). Additionally, *Xcl1* was also upregulated in the T_M population (Figure 3A), which might lead to the attraction of $XCR1^+$ dendritic cells located in the white pulp (Yamazaki et al., 2013), potentially contributing to the generation of secondary effector cells (Argilaguet et al., 2019 Im et al., 2016). T_M cells also expressed higher levels of *Cxcl10* (Figure 3A) and its receptor *Cxcr3* (Figure 3B), with CXCL10 being reported to be upregulated in newly activated CD8 T cells and CXCR3 being needed for clonal expansion (Peperzak et al., 2013). Finally, T_M cells expressed higher levels of the co-stimulatory receptor *Icos* (Figure 3C), important in maintenance of high numbers of cytotoxic CD8 T cells during infection (Bertram et al., 2002), and higher levels of *Cxcr4* (Figure 3B), relevant for memory T cell homeostatic maintenance in the absence of antigen (Chaix et al., 2014). Regarding transcripts relevant for cytotoxic functions, T_M cells had low counts, but both T_E and T_{Exh} expressed elevated levels. Specifically, *Gzma* and *Gzmk* were predominantly expressed in T_{Exh}, whereas *Prf1* and *Gzmb* exhibited higher expression levels in T_E cells (Figure 3A).

The third factor ordered the cells along an effector-to-exhaustion axis, identifying three distinct phenotypes: T_E, T_I, and T_{Exh}. Genes positively correlated with the third factor were significantly enriched in exhaustion-associated markers, whereas the genes negatively correlated with this factor were significantly enriched in effector genes (Figure 2I). T_E (denoted by clusters 1, 8, and 9) cells were mostly found in the lung, blood, and spleen (Figure 2J) and had high levels of transcription factors associated with an effector program, such as *Klf2*, *Zeb2*, and *Tbx21* (encoding T-bet) (Dominguez et al., 2015), high *Cx3cr1* (Gerlach et al., 2016) and *Gzmb* expression (Ebnet et al., 1991), and high expression of NK receptors, such as *Klre1* (Westgaard et al., 2003) and *Klrk1* (Groh et al., 2001; Figure 2M).

T_{Exh}, composed of clusters 0, 2–5, and 11–12, were found in all tissues at different frequencies and made up most cells found in peripheral tissues (BM and liver) with the exception of lungs (Figure 2J). T_{Exh} cells were characterized by higher expression of inhibitory receptors *Pdcd1* (encoding PD-1), *Cd160*, *Cd244*, *Lag3*, *Eomes*, and chemokine receptor *Cxcr6* (Figure 2N).

The T_I population, composed of clusters 6 and 13 and present in all tissues (Figure 2J), had features of both T_E and T_{Exh} phenotypes. Previous studies showed that T_{Exh} cells co-express multiple co-inhibitory receptors, a high Eomes-to-T-bet ratio (Paley et al., 2013), and high levels of the master regulator TOX (Alfei et al., 2019; Khan et al., 2019; Yao et al., 2019). Accordingly, *Tox* transcripts were more abundant in T_{Exh} cells than in T_E cells. Additionally, compared with T_E cells, T_{Exh} cells were defined by higher expression of the inhibitory receptors *Pdcd1*, *Cd160*, *Cd244, Cd200r1*, and *Lag3* (Figure 3D) and chemokine receptors *Cxcr3* and *Cxcr6* (Figure 3B). CXCR3 is relevant for migration of effector CD8 T cells into tissues by sensing its ligands CXCL9/CXCL10 (Hu et al., 2011). CXCR6 ligand (CXCL16) is constitutively expressed in the liver, lungs, spleen, and LNs (Matloubian et al., 2000), and it is also upregulated on fibroblasts and vascular cells by pro-inflammatory cytokines, such as IFN-γ and TNF-α (Abel et al., 2004). Another transcript highly expressed was *Cd7* (Figure 3D), previously described to be upregulated in virus-specific CD8 T cells in chronic LCMV infection (Erickson et al., 2015; Doering et al., 2012), possibly promoting cytotoxic responses (Lee et al., 1998).

T_{Exh} cells exhibited higher *Il21r* expression (Figure 3E) and the IL-21-induced transcription factor *Batf* (Figure 3D). During advanced chronic LCMV infection, IL-21 plays a critical role for the maintenance and function of virus-specific CD8 T cells via a basic leucine zipper transcription factor (BATF)-mediated transcriptional program (Xin et al., 2015; Yi et al., 2009; Fröhlich et al., 2009). As opposed to the T_E cells, T_{Exh} cells expressed lower *Il18r1* and *Il18rap*, encoding IL-18 receptor (IL-18R) and its accessory protein, respectively (Figure 3E), which correlate with poor effector functions (Ingram et al., 2011). Among T_{Exh}, cluster 11 was composed of P14 isolated from all tissues (Figure 1E) and had a very strong IFN-related signature (Table S2; Figure S2). This cluster also had the highest expression of type I IFN-regulating master transcription factor *Irf7*, whose transcription is controlled by ISGF3, composed of transcription factors *Stat1*, *Stat2*, and *Irf9* (Sato et al., 1998), which were also upregulated (Table S1). Moreover, *Stat1* and *Stat2* targets were also upregulated (Table S2). This cluster had also upregulated expression of IFN-induced chemokine CXCL10 (Farber, 1997; Figure 3A). This signature might be a result of close interaction of P14 cells with recently infected, type I IFN-producing cells.

(J) Phenotypic composition of P14 cells isolated from various tissues with respect to functional phenotypes.
(K–N) Violin plots of selected markers correlating strongly with the defined functional phenotype: P, proliferating (K); M, memory-like (L); E, effector-like (M); and Exh, advanced exhaustion (N).

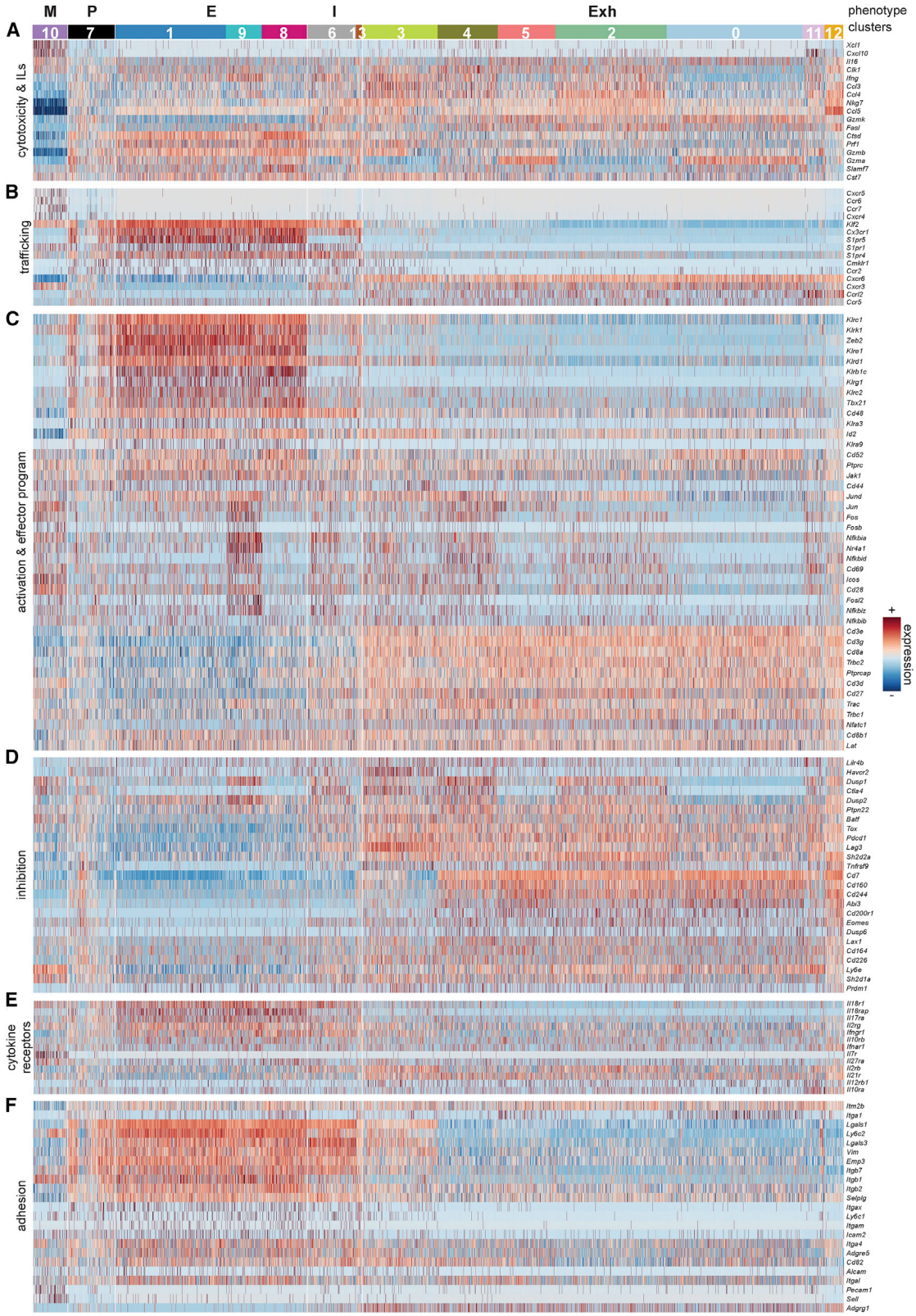

(legend on next page)

Taken together, T_{Exh} cells expressed cytokine receptors such as IL-21R being critical for their survival and subsets thereof might be more exposed to type 1 IFN signals than most T_{Exh} or T_M cells.

The expression pattern of inhibitory receptors varied within the T_{Exh} cells. For example, cluster 3 in particular had higher *Havcr2*, *Lag3*, and *Ctla4*, but lower *Cd160* and *Cd244* compared with the rest of the cells within T_{Exh} phenotype (Figure 3D). Besides TCR activation, specific cytokines are required for some co-inhibitory receptors' upregulation and/or maintenance. IL-2 and/or IL-15 stimulation is essential for upregulation of TIM-3, 2B4, and maintenance of LAG-3 (Beltra et al., 2016). Cluster 3 had also elevated *Il2rb* (Figure 3E), encoding CD122, the common subunit of the IL-15R and IL-2R. Moreover, the cells from this cluster originated from lungs and LNs, which are two tissues shown to retain injected IL-15 (Sato et al., 2007) and express IL-15 in naive mice (Baumann et al., 2018). Within T_{Exh} cells, the liver-specific cluster 0 was characterized by the lowest levels of *Nr4a1* encoding NUR77, *Nfkbid*, and activator protein 1 (AP-1) transcripts *Jun* and *Jund* (Figure 3C), suggesting very low TCR activation. Clusters 2 and 12 were BM specific. Both populations showed enrichment in four genes (*Ngp*, *Camp*, *S110a9*, *S110a8*) (Table S1), which have been predicted to be part of a degranulation pathway (Szklarczyk et al., 2019), suggesting this pathway might be specifically induced in BM. Compared with cluster 12, cluster 2 had lower *Ctla4* and more *Gzma* (Figures 3D and 3F). Cluster 4 was spleen specific and, compared with the other T_{Exh} clusters, had increased nuclear factor κB (NF-κB) transcripts and *Junb*. Cluster 5 was composed of cells mainly isolated from the blood and expressed high *Gzma* (Figure 3A).

T_E cells expressed high levels of *Cx3cr1* (Figure 3B), a chemokine receptor associated with a terminally differentiated effector phenotype (Gerlach et al., 2016), and transcription factors supporting an effector program, including *Tbx21* (encoding T-bet), *Zeb2*, and *Id2* (Dominguez et al., 2015, Knell et al., 2013; Figure 3C). As opposed to T_{Exh} cells, they expressed lower levels of co-inhibitory receptors (Figure 3D). Furthermore, they expressed many adhesion molecules, such as *Itgb7*, *Emp3*, *Itgax*, *Itgb1*, *Itgb2*, *Itgal*, and *Itga4* (Figure 3F), important in adhesion to the vasculature and extravasation of activated T cells into tissues (Andersson et al., 1995, Christensen et al., 1995). Moreover, the T_E cells expressed higher levels of CD11b (encoded by *Itgb2* and *Itgam*) and CD11c (encoded by *Itgb2* and *Itgax*), both being markers expressed on effector CD8 cells with high cytotoxic potential upon recent activation (Christensen et al., 2001; Lin et al., 2003). T_E cells also had higher expression of Ly6c (Figure 3F), a surface molecule important in lymphocyte-endothelial adhesion, usually expressed by memory CD8 T cells (Walunas et al., 1995). Furthermore, T_E cells showed higher expression of *Klf2* and its target, *S1pr1* (Figure 3B). *S1pr1* and *S1pr4* (also upregulated) are important in tissue egress (Skon et al., 2013).

T_E from cluster 9 (with the majority of cells harvested from spleen, but also lung and LNs) had the most activated cells based on expression of *Nr4a1* encoding NUR77 (as a proxy for TCR signaling) (Moran et al., 2011; Ashouri and Weiss, 2017). Consistent with this observation, AP-1 and NF-κB transcription factors (*Jun*, *Jund*, *Nfkbiz*, *Nfbid*) were also upregulated, suggesting that these cells have recently been exposed to antigen. Additionally, target genes of *Fos*, *Jun*, *Jund*, and *Fosl2* were also upregulated (Table S2). Among the T_E cells, cluster 8, mainly isolated from the blood, expressed lower *Nr4a1* and *Cd69*, which is to be expected for circulating cells because they are probably not in contact with infected cells. Compared with T_E cells, T_{Exh} cells exhibited higher levels of TCR genes and associated surface molecules, such as CD3 and CD8 (Figure 3C). CD8 T cells downregulate TCR genes and TCR-associated genes following activation (Paillard et al., 1990), suggesting that cells displaying a more exhausted phenotype (compared with T_E cells) were less activated. Taken together, T_E cells exhibited a more activated gene expression signature compared with T_{Exh} cells, potentially because of stronger co-inhibition of the latter.

T_I phenotype had features of both T_{Exh} and T_E cells (Figures 3B and 3C), suggesting that one of these subsets might differentiate into the other. These cells had intermediate transcript levels of *Cx3cr1*, *Zeb2*, and inhibitory receptors *Pdcd1* encoding PD-1, *Lag3*, and *Cd160*. Moreover, cells from this cluster had elevated *Nr4a1* encoding NUR77, suggesting they had recently encountered antigen (Figure 3C). It is therefore likely that the cells exhibiting a T_I phenotype are in transition either toward a T_{Exh} or T_E phenotype.

Validation of the Functional Phenotypes by Flow Cytometry

Having established, based on the scRNA-seq profile, five functional phenotypes of P14 cells contributing in various proportions to the overall population of cells found in specific tissues, we next validated these results by staining P14 cells for specific key markers that were differentially expressed in the five functional phenotypes (Figures 4A–4N). Specifically, T_{Exh} cells (PD-1^{hi} $CXCR3^{hi}$ $CXCR6^{hi}$) exhibited lower levels of CX3CR1 (Figures 4A–4C), a marker identifying the T_E population. Also, P14 cells harvested from blood, liver, and BM, expressing the highest levels of PD-1, CXCR6, and CXCR3 (Figure 4K), also contained the highest frequencies of T_{Exh} cells on the transcriptional level.

The T_E population was demarcated by high expression of CX3CR1, was most abundant in the lung, and showed low expression of PD-1 (Figure 4L). Furthermore, $CXC3CR1^{hi}$ expressed low levels of the key exhaustion transcription factor TOX (Figures S3A and S3B) and high levels of GZMB (Figures 4D and S3C), confirming the scRNA-seq data. Moreover, there was a trend toward higher IFN-γ expression frequencies of CD8 T cells following *in vitro* restimulation in sorted P14 cells from organs having the lowest frequencies of the T_{Exh} phenotype (Figure 4E). Of note, irrespective of the tissue of origin, all P14 cells showed high degranulation levels (Figure 4E), consistent

Figure 3. Heatmap Showing Normalized Expression of Relevant Genes for Assignment to Functional P14 Clusters

Colors indicate cluster assignment shown in Figure 1B. The phenotype refers to the functional phenotype: E (effector-like), I (intermediate), Exh (advanced exhaustion), P (proliferating), and M (memory-like). Genes were grouped by biological function: secreted ILs and cytotoxicity (A), trafficking (B), activation of TCR and genes associated with effector phenotype (C), inhibition of TCR signaling (D), IL receptors (E), and adhesion (F). Rows from each group were hierarchically clustered based on gene expression. See also Tables S1 and S2 and Figure S2.

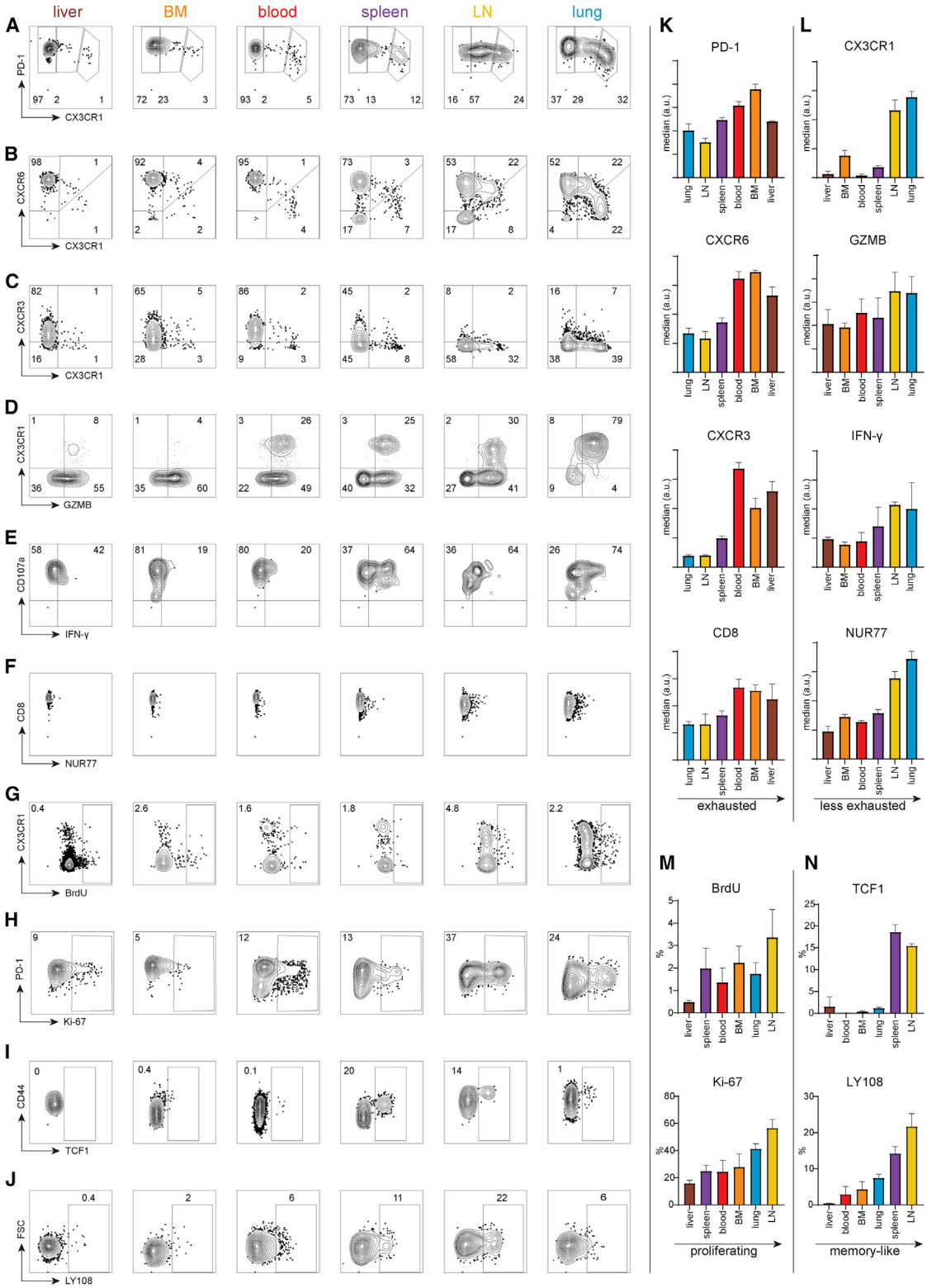

Figure 4. Experimental Validation (Protein Staining) of the Five Functional Phenotypes Based on the Transcriptomic Profile

(A–J) Examples of flow cytometry plots showing the profile of relevant markers for phenotype identification.

(K and L) Medians of virus-specific cells expressing proteins associated with T_{Exh} (K) or T_E phenotype (L).

(legend continued on next page)

with previous studies reporting efficient *in vivo* and *in vitro* killing of pulsed naive targets by exhausted cells (Agnellini et al., 2007; Richter et al., 2010; Graw et al., 2011). Organs with high frequencies of less exhausted cells (such as lungs, LNs, and spleen) had the highest NUR77 levels (Figure 4F), indicative of productive TCR engagement (Ashouri and Weiss, 2017). In contrast, an opposite trend was observed with respect to CD8 expression (Figures 4H and 4K), suggesting that cells isolated from more exhausted organs (such as blood, BM, and liver) received less TCR stimulation (Paillard et al., 1990).

The fraction of cycling cells was highest in LNs and lungs (Figure 4M). A single bromodeoxyuridine (BrdU) pulse 12 h prior to sacrifice confirmed that the fraction of P14 cells actively proliferating (cluster 7) was low in all tissues (Figures 4G and 4H), also evidenced by Ki-67 staining (Gerdes et al., 1984).

T_M cells (cluster 10), found mainly in the LNs and spleen (Figure 4N), as shown previously (Utzschneider et al., 2016b), were identified by TCF1 expression (Figure 4I) and the expression of the surface protein LY108 (encoded by *Slamf6*) (Figure 4J).

Effector-like Cells Localize Close to the Vasculature

T_E cells exhibited a distinct transcriptional pattern compared with T_{Exh} cells, expressing many adhesion molecules and the sphingosine receptor *S1pr1*. We hypothesized that these cells are located close to the vasculature because cells residing in tissues do not express S1PR1, and most of the cells displaying a T_E phenotype were found in the lungs, but not in other peripheral tissues. To test this hypothesis, we performed an intravascular *in vivo* labeling with an α-CD8 antibody prior to sacrifice to assess tissue localization (Figure 5A). T_E cells, identified by high CX3CR1 expression, were indeed found exclusively within/close to the vasculature as indicated by their positive intravascular staining (Figure 5B). CX3CL1 (fractalkine), the CX3CR1 ligand, was found to be expressed by endothelial and epithelial cells (Pan et al., 1997; Fong et al., 1998), which might explain why so many T_E cells were found in the lungs, a highly vascularized organ. Moreover, T_E cells had lower PD-1 expression (Figure 5A), suggesting that they received less TCR stimulation compared with their $CXC3CR1^{lo}$ counterparts in tissues exhibiting higher PD-1 expression.

The Phenotype of P14 Cells Is Plastic

Protein measurements and scRNA-seq data suggested that P14 cells adopted functional phenotypes differentially represented in tissues. We aimed at investigating whether there was tissue-specific homing of phenotypes and whether the phenotype of these cells was imprinted or plastic. P14 cells isolated from four organs harvested 14 days post infection (dpi) were separately adoptively transferred into chronically infected hosts and analyzed in the same four organs 1 week later with respect to their numbers and phenotype (Figures S4 and S5). The re-isolated P14 cells adopted in their new host a tissue-specific phenotype alike the one of the endogenous pool CD8 cells. P14 cells isolated from lungs and liver could be grouped by organ of recovery rather than tissue of origin (Figures S4D–S4H; Figures S5D–S5G), suggesting the observed phenotype was determined by the organ of recovery. Additional markers (such as PD-1, CD44, and NUR77) were also differentially expressed in cells that had the same origin, but were harvested from different tissues after adoptive transfer (Figures S4H and S4I). There are two hypotheses that could explain these observations. The transferred cells could either be plastic or preferentially home to a specific tissue, depending on their phenotype. Given the fact that the transferred cells did not preferentially home to a particular tissue (Figure S4J), the first hypothesis based on plasticity is favored. In fact, irrespective of their origin, the highest frequencies of transferred cells were found in the lungs. Moreover, the number of recovered cells was highest for transferred cells initially isolated from the lungs, which had the highest frequency of T_E cells, and lowest for cells originally isolated from the liver, which had predominantly an advanced exhaustion phenotype (Figure S4K).

Functional Phenotypes Are Plastic 14 Days into Chronic LCMV Infection

Because the P14 populations were heterogeneous at the time of secondary transfer into chronically infected hosts (Figures S4B and S5B), the observed plasticity could have been because of preferential retention of a subset in a particular tissue. Next, we aimed at assessing the plasticity of homogeneous sorted populations. P14 cells were sorted from chronically infected mice 14 dpi based on TCF1, CXCR6, and CX3CR1 expression to isolate T_M, T_E, T_I, and T_{Exh} subsets. These sorted populations were separately transferred into infection-matched hosts. One week later, animals were sacrificed and P14 cells were isolated from spleen, lung, and liver (Figure 6A). All transferred populations changed their phenotype depending on the tissue of recovery, but to a different extent. All cells found in the liver, regardless of their tissue origin, expressed CXCR6 to some degree, whereas at least a fraction of cells harvested from lung and spleen expressed CX3CR1 (Figures 6B and 6C). Nevertheless, the functional phenotype of the transferred population had a very strong influence on the observed phenotype. This effect was independent of the tissue of origin (Figures 6B and 6C). T_E populations partially maintained a high CX3CR1 and low CXCR6 expression. However, in lung and liver in particular, CX3CR1 downregulation and CXCR6 upregulation were clearly visible. Inversely, T_{Exh} cells were capable of upregulating CX3CR1, especially when found in the spleen (Figure 6C). The highest degree of plasticity, based on only CXCR6 and CX3CR1 or all measured markers, was displayed by the intermediate population (Figures 6B and 6C). When found in the liver, these cells expressed high CXCR6 and downregulated

(M and N) Frequency of cells positive for cell-cycle-related marker Ki-67 and BrdU incorporation (M) or transcription factor TCF1 and surface marker LY108 associated with the T_M phenotype (N). Samples were ordered on the x axis based on the functional phenotype frequency from the transcriptional analysis shown in (A).

Regarding the degree of exhaustion (K and L), cells isolated from blood and spleen had similar frequencies of the T_{Exh} population. Because the spleen had a higher frequency of T_M cells, it was considered "less exhausted" than the blood. Representative data from at least two independent experiments are shown (n = at least 2 mice). Bar plots show mean ± SD. See also Figure S3.

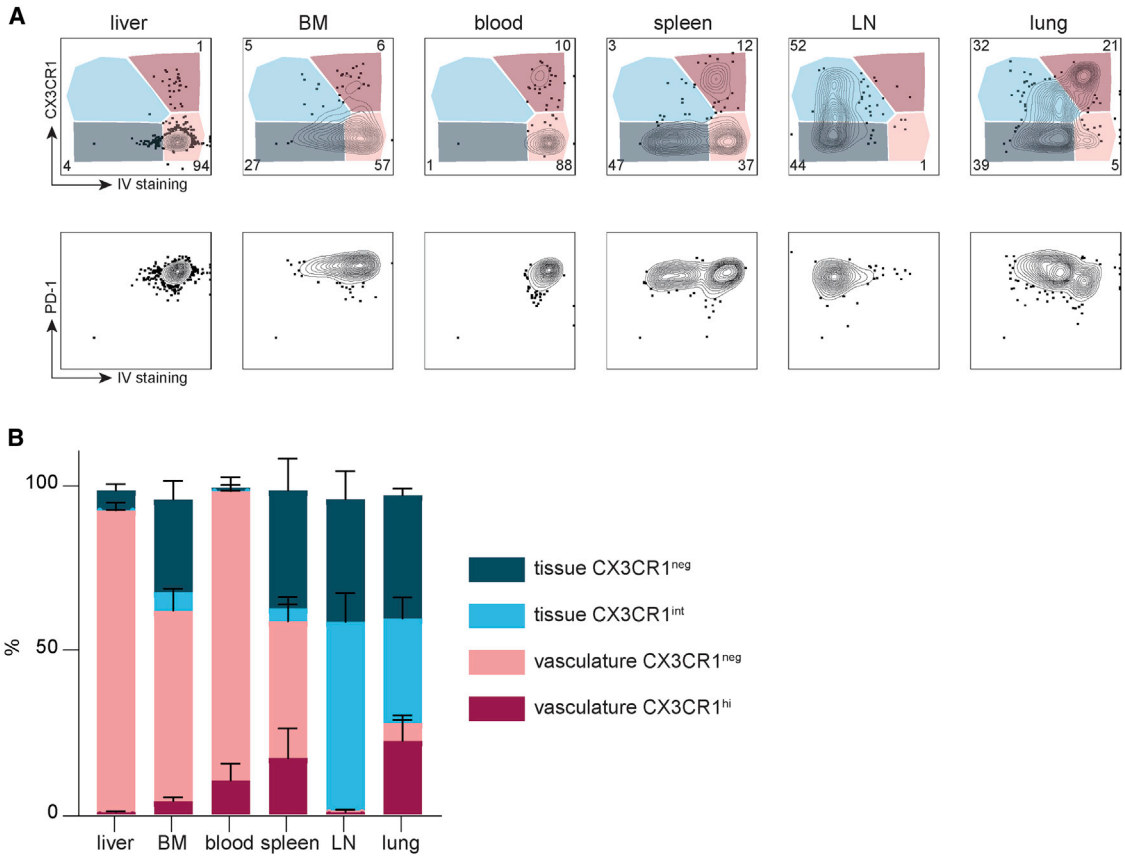

Figure 5. Localization of Effector-like P14 Cells

Intravascular or within-tissue localization was assessed 3 weeks into chronic LCMV infection by intravenous administration of anti-CD8 antibody shortly before cell harvesting and additional *in vitro* staining.

(A) Representative flow cytometry plots of P14 cells isolated from different tissues following CD8 intravascular staining.

(B) Contribution of the four populations defined in (A) to each tissue sample. Representative data from two independent experiments are shown (n = 3 mice). Bar plots show mean ± SD.

CX3CR1, whereas in the lung and spleen, CX3CR1 was still expressed. Interestingly, T_M cells did not upregulate CX3CR1 in any tissue, upregulated CXCR6 in spleen and lungs, and to a large extent, maintained TCF1 expression (Figure 6B). Moreover, the T_{Exh} CXCR6^{hi} populations maintained a relatively high CXCR6 expression and had higher PD-1 and CD39 expression, particularly when harvested from the liver, whereas T_E CX3CR1^{hi} maintained high CX3CR1 and KLRG1 expression (Figure 6B). Consistent with previous observations, irrespective of the functional phenotype, the majority of the cells were found in the lung. There was, however, a slight increase of cells found in the spleen when the transferred population had a T_E phenotype (Figure 6D).

T_I Cells Maintain Plasticity 21 Days into Chronic LCMV Infection

Next, we investigated whether the observed plasticity of the functional phenotypes was maintained over time. Using the same experimental setup as before, we sorted P14 cells from chronically infected mice 21 dpi and transferred them into infection-matched hosts. One week later, animals were sacrificed and P14 cells were isolated from spleen, lung, and liver (Figure S6A). T_{Exh} and T_E cells maintained their phenotype (Figures S6B and S6C). Only the T_I population showed plasticity with respect to CXCR6 and CX3CR1 and other measured markers (Figure S6B); in the liver, T_I cells were CXCR6^{hi} CX3CR1^{lo}, whereas in spleen and lungs, they gave rise to a CXCR6^{int}CX3CR1^{hi} population, resembling T_E cells (Figure S6C). T_M cells in the spleen and, to some extent, in the lungs maintained high TCF1. Transferred cells were most frequently found in the lungs, irrespective of their origin. However, there was a slight tendency for T_E cells to be more prevalent in the spleen and for T_{Exh} cells to be enriched in the liver (Figure S6D). Overall, there is less plasticity observed 21 dpi than at 14 dpi.

T_E and T_I Cells Exhibit Better Re-expansion Potential Than T_{Exh} Cells

Next, we assessed the fitness of the functional phenotypes in the absence of a chronic environment. P14 cells harvested from lung, spleen, or liver of chronically infected mice 21 dpi were sorted into TCF1^{hi} T_M, CX3CR1^{hi} T_E, CX3CR1^{int} T_I, and CXCR6^{hi}CX3CR1^{lo} T_{Exh} and transferred into naive hosts, which

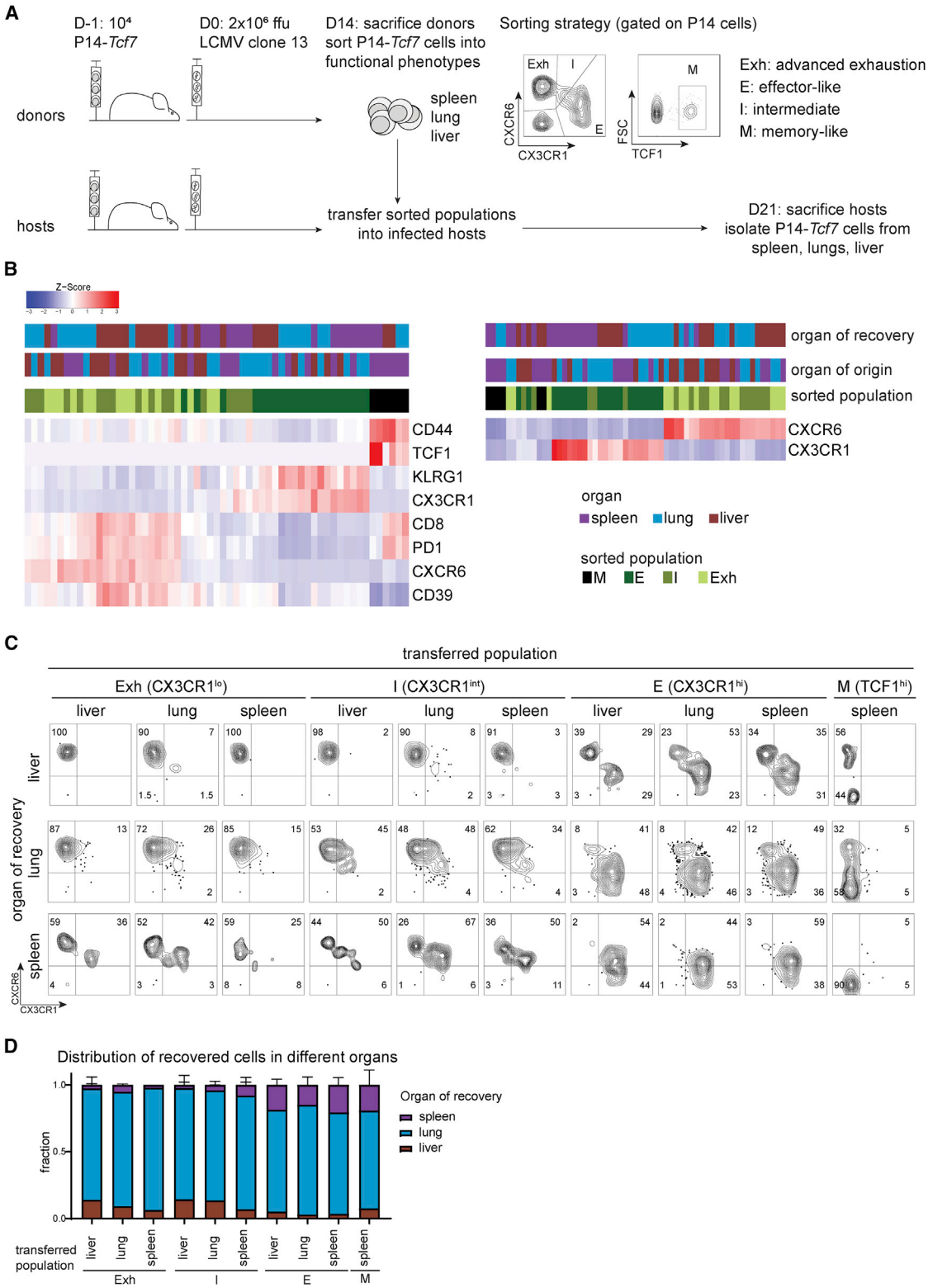

Figure 6. Plasticity of Sorted Functional Populations 14 Days into Chronic Infection

(A) Experimental setup.

(B) Heatmaps showing marker expression of isolated cells. The samples were clustered based on median expression of markers shown on the right. Only samples containing more than 50 P14 cells were considered.

(legend continued on next page)

were infected with a low dose of LCMV the following day. One week later, the animals were sacrificed and spleens were harvested for analysis (Figure 7A). T_M cells had the highest re-expansion rate, whereas T_{Exh} cells had the lowest. T_I and T_E cells were recovered in higher numbers than T_{Exh} cells, but substantially lower than T_M cells (Figures 7B and 7C). Interestingly, the phenotype of the cells in the new hosts was strongly influenced by the functional phenotype acquired in the chronically infected donors. In the new hosts, T_E cells had higher CX3CR1 and KLRG1 expression, whereas T_{Exh} cells had higher CXCR6 expression (Figures 7D and 7E). Clustering based on CXCR6 and CX3CR1 or all measured markers grouped the samples by the functional phenotype (Figure 7D). In the new recipients, T_M cells gave rise to all phenotypes, whereas the other functional phenotypes (T_E, T_I, and T_{Exh}) differentiated into both CX3CR1^{hi}CXCR6^{int} and CX3CR1^{lo}CXCR6^{hi} populations, but in different ratios (Figure 7E).

DISCUSSION

We have characterized the landscape of exhausted P14 cells isolated from six tissues (blood, spleen, BM, LNs, lungs, and liver) harvested from mice chronically infected with LCMV clone 13 and classified them into five main functional phenotypes: T_M, T_P, T_E, T_I, and T_{Exh}. Clusters 10 (T_M) and 7 (T_P) could be easily identified by TCF1 staining and BrdU incorporation, respectively, whereas CXCR6 and CX3CR1 discriminated between T_E (CX3CR1^{hi}), T_I (CX3CR1^{int}), and T_{Exh} (CX3CR1^{lo}CXCR6^{hi}). T_M cells expressed TCF1 and were found only in LNs and spleen, as previously reported (Utzschneider et al., 2016b; Im et al., 2016). The highest frequency of T_P cells was in the LNs, where a significant T_M population was also located. However, T_P cells could be found in all other tissues in lower frequencies, implying P14 cells actively divide, albeit to a low extent, both in the periphery and lymphoid organs. Protein staining confirmed that CX3CR1^{hi} T_E cells were found mostly in the lungs, but also spleen and blood. Moreover, T_E phenotype matched the transcriptional profile: CX3CR1^{hi} and PD-1^{lo} cells were also GZMB^{hi}, CXCR6^{lo}, and CXCR3^{lo}. T_E cells expressed many adhesion transcripts (*Itgb7*, *Emp3*, *Itgax*, *Itgb1*, *Itgb2*, *Itgal*, *Itga4*) and were located close to the vasculature, suggesting that they might be in the process of extravasation. PD-1^{hi} CXCR6^{hi} T_{Exh} cells were found in all screened tissues. The T_I population was observed in all tissues, with LNs exhibiting the highest frequency. T_I shared both T_E and T_{Exh} features, indicating potential conversion of one subset into another. This population had also higher *Nr4a1* expression, a marker of recent TCR signaling (Moran et al., 2011). Exhaustion is a gradual process, triggered by persistent antigen stimulation (Bucks et al., 2009; Utzschneider et al., 2016a; Angelosanto et al., 2012; Beltra et al., 2020). The expression of co-inhibitory receptors is positively correlated with TCR signaling, which means T_{Exh} cells were more stimulated than T_E cells. If the development of terminal exhaustion is a linear process (Beltra et al., 2020), and because the transcriptional profile of T_E cells appears the most functional, T_M cells might give rise to T_E cells, which in turn might develop into T_{Exh} with persistent TCR stimulation. In this scenario, T_I cells might be a "bridging population" in the T_M-T_E-T_{Exh} differentiation axis. This would implicate that CX3CR1^{hi} cells from a chronic infection setup are different from the ones described in the context of acute LCMV infection, where they were described as terminally differentiated (Gerlach et al., 2016). Recent studies showed that there is a TCF1-controlled bifurcation early in chronic exhaustion, leading to terminally differentiated effector-like KLRG1^{hi} cells, which are not sustained long-term, and to exhausted cell precursors, which are able to survive better (Chen et al., 2019). In our experimental setting, T_E cells re-expanded better than T_{Exh} cells after re-exposure to LCMV in a naive host. One possibility that might explain this difference is the timing of analyses. Chen et al. (2019) analyzed cells during the early phase of chronic infection (day 8) compared with days 14–21 in our case. The seemingly contradictory results suggest that the T_E population we identified may be phenotypically and functionally different from the one described in the early stages of exhaustion. Recent studies (Zander et al., 2019; Hudson et al., 2019) described T_E cell populations during later stages of chronic LCMV infection (day 28 or later), displaying a similar transcriptional profile to our data, and showed that these cells are functionally better than T_M or T_{Exh} cells. Our results are consistent with Zander et al. (2019), who performed adoptive transfer experiments of sorted homogeneous populations based on CX3CR1 and LY108 expression and showed that T_E cells are fitter than T_{Exh} cells, and that the phenotypes of these populations were strongly influenced by the acquired phenotype before sort, but were plastic to some degree.

Another surprising finding was the plasticity of P14 cells in chronic infection, in particular the T_E cells, which were able to downregulate CX3CR1. Adoptive transfer experiments performed in the setting of an acute LCMV infection clearly showed that CX3CR1^{hi} cells cannot give rise to CXC3CR1^{int} or CXC3CR1$^{low/neg}$ cells, prompting the idea that CX3CR1 expression correlates with terminal effector differentiation (Gerlach et al., 2016). When CX3CR1^{hi} cells were transferred into chronically infected mice and recovered from tissues with a strong T_{Exh} signature, such as the liver, CX3CR1 was downregulated in a substantial fraction of the recovered cells. When CX3CR1^{hi} cells were recovered from the spleens of chronically or acutely infected hosts, most cells maintained a high CX3CR1 expression. Also, compared with T_M or T_E cells developed in acute infection, exhausted cells have a different transcriptional and epigenetic program (Khan et al., 2019; Chen et al., 2019; Doering et al., 2012; Wherry et al., 2007), which might explain the (potentially) different regulation of CX3CR1.

P14 cells isolated from LNs, spleen, and lungs were the most heterogeneous, with at least two clusters making up at least 10% of the population. Cells from the blood were mainly split into two clusters, while P14 cells harvested from BM and liver were the most homogeneous samples. In fact, the landscape of

(C) Representative flow cytometry plots (n = 2–3 mice) showing expression of CXCR6 and CX3CR1 (gated on P14-Tcf7 cells).
(D) Distribution of recovered P14 cells in different tissues denoted by color. Bar plots show mean ± SD. One of two experiments is shown.
See also Figures S4 and S5.

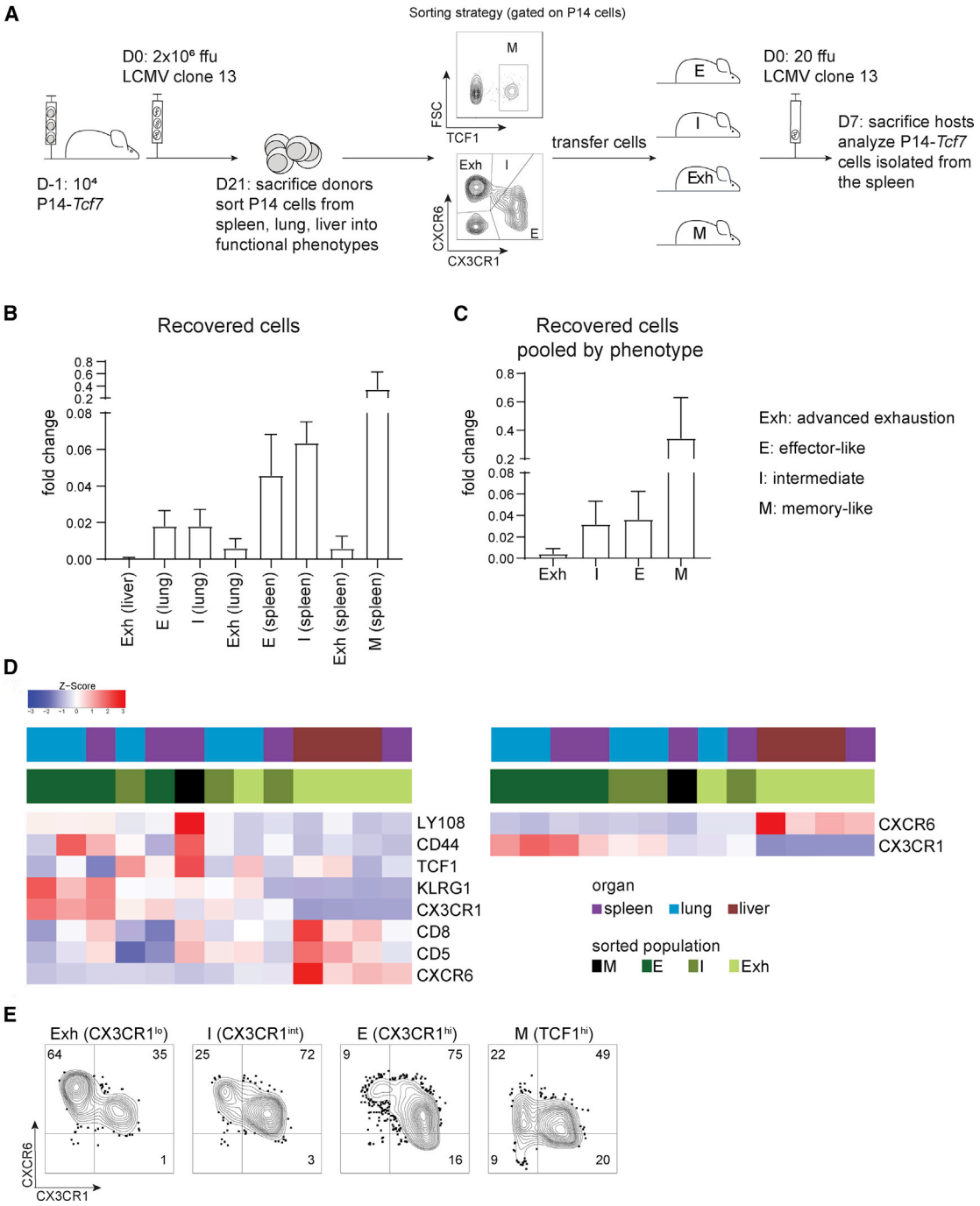

Figure 7. Fitness of the Functional Phenotypes

(A) Experimental setup.

(B and C) Recovered cells from spleen in each group, defined by functional phenotype and origin of transferred cells (B) (n = 3 mice) or only functional phenotype (C). Bar plots show mean ± SD.

(D) Heatmaps showing marker expression of isolated cells. The samples were clustered based on median expression of all markers measured (left) or just CXCR6 and CX3CR1 (right) (n = 1–3 mice).

(E) Representative flow cytometry plots showing expression of CXCR6 and CX3CR1 (gated on P14-Tcf7 cells isolated from the spleen). One of two experiments is shown.

See also Figure S6.

exhausted cells might be even more diverse with respect to heterogeneity of lowly expressed genes. The droplet sequencing technique results in noisy expression profiles, with a high rate of dropouts, particularly impeding the detection of lowly expressed genes (Svensson et al., 2017). Expression profiling in general is imperfectly correlated with protein expression (e.g., IFN-γ) (Mackerness et al., 2010). Moreover, transcripts do not necessarily result in active proteins because post-transcriptional regulation and/or post-translational modifications may be required (Mann and Jensen, 2003). The experimental setup without technical and individual biological replicates does not allow to properly control for batch effects. In this study, cells harvested from three mice were pooled before sequencing to make sure the results are representative. Furthermore, the lysis and transcript amplification of all six samples were performed the same day. Eight of 14 clusters were composed of more than 80% cells isolated from one tissue only. However, the remaining six clusters were mixed with three clusters containing cells from all six organs, suggesting that these cells share the same phenotype and that the batch effects were weak in this case. Also, cells isolated from LNs do not make up more than 80% of any cluster, meaning that there was no LN-specific cluster. However, the assessment of batch effect is not possible due to the experimental design, which does not allow to assess the performance of any type of batch correction method because we do not have a control population (such as a common population among all tissues). Importantly, cells from different tissues (mainly spleen and LNs) exhibiting a strong T_M phenotype previously described (Utzschneider et al., 2016b) were grouped together based on clustering of uncorrected data, suggesting that (at least for this population) the batch effects were minimal. We applied Harmony batch correction (Korsunsky et al., 2019), which performed best on a test dataset (data not shown). Reassuringly, even after batch correction, the five main functional phenotypes were still maintained (Figure S7). However, clusters from different tissues having the same functional phenotype (T_E or T_{Exh}) were mixed after batch correction (Figure S7C). In addition, the frequencies of the T_M population were closer to the expected ones (based on phenotypic characterization of this cell subset in various tissues by flow cytometry) (Figure S7H) in the uncorrected data than in batch-corrected data (Figure S7I), raising some concerns about the suitability of batch correction for our dataset. Finally, to evaluate whether the qualitative differences highlighted in Figures 2 and 3 with respect to the five phenotypes are preserved irrespective of any potential batch effect, we performed differential gene expression analyses between the main phenotypes within each individual tissue sample. We then compared the union of these gene sets with the list of genes we previously identified as being differentially expressed with respect to the main phenotypes (most genes in Figure 3, which are discussed in the manuscript). All genes found to be differentially expressed contributing to the main phenotypes' signatures were included in the union of gene sets. Overall, the differences between the main functional phenotypes are preserved irrespective of batch correction.

We found that half of the clusters were tissue specific. This observation indicates that exhausted cells adopt tissue-specific transcriptional signatures, suggesting the microenvironment is important in shaping the phenotype of P14 cells in chronic infection. Because these cells were isolated from various organs with distinct types of infected cells and inflammatory milieu, it is not surprising that these cells adopted tissue-specific phenotypes. For instance, regardless of their T_E or T_{Exh} phenotype, cells harvested from the spleen had higher expression of *Nr4a1*, *Nfkbid*, and *Nfkbiz*, whereas cells isolated from the blood had low expression of these transcripts, indicating that P14 cells from the spleen recently encountered their antigen, whereas circulating cells did not. P14 cells isolated from the liver also had the lowest TCR signaling and *Ifng* expression, but high *Gzma*. Expression of specific chemokine receptor transcripts correlated with different functional phenotypes. *Ccr7* and *Sell* expression, detected in the $TCF1^+$ T_M cells, could explain why these cells were found in secondary lymphoid organs. CX3CR1 was highly expressed in T_E cells, which were found only close to the vasculature and not deeper in peripheral tissues. T_E cells were most abundant in the lung, an organ that is highly vascularized and exhibits high levels of its ligand CX3CL1. Circulating P14 cells isolated from blood had both T_E and T_{Exh} phenotypes. CXCR6 and CXCR3 expression was more abundant in T_{Exh} cells, preferentially localized deeper in the tissues. High inhibitory receptor expression in T_{Exh} cells is an indicator of repeated TCR stimulation likely occurring in the tissues, which might be beneficial to the host by limiting immunopathology (Frebel et al., 2012; Frebel and Oxenius, 2013).

Adoptive transfer of bulk P14 cells harvested from different organs into chronically infected hosts did not show any tissue-specific homing and suggested that the tissue-specific phenotype was plastic. However, because tissue populations were heterogeneous, we decided to transfer homogeneous P14 populations of sorted T_M, T_E, T_I, or T_{Exh} subsets. Although there was a strong influence of the initial phenotype acquired in the chronically infected donors, the functional phenotypes were able to partially modulate the expression of CX3CR1 and CXCR6, depending on the tissue of recovery when cells were sorted 14 days into chronic infection. However, when cells were isolated 21 days into chronic infection, the T_E and T_{Exh} populations hardly changed, while the T_I population displayed the same plasticity observed 1 week earlier, giving rise to both T_E and T_{Exh} populations. Additionally, the global phenotype of P14 cells isolated from different tissues did not correlate with viral titers. For example, the spleen and liver were shown to have similar viral kinetics (Wherry et al., 2003), but the P14 cells isolated from these organs displayed strikingly different phenotypes: the majority of cells from the liver were T_{Exh} cells, whereas P14 cells from the spleen were very diverse. These data suggest that T cell differentiation in chronic infections is impacted by both cell-intrinsic and -extrinsic features, which are gradually more stable over the course of the infection, and tissue-driven changes resulting from niche-specific differences.

Recent studies (Zander et al., 2019; Hudson et al., 2019) showed that T_E cells are functionally superior compared with T_M or T_{Exh} cells. Despite secreting less IFN-γ and IL-2 compared with functional memory or effector cells generated in an acute infection, exhausted cells still have cytotoxic potential because they are able to efficiently kill pulsed naive target cells *in vivo* (Agnellini et al., 2007; Graw et al., 2011). However, these naive

targets do not highly express ligands recognized by co-inhibitory receptors, which are highly upregulated on exhausted cells in chronic infection. This might in part explain why exhausted cells do not efficiently eliminate infected cells within a chronically infected host. Moreover, in line with previous studies (Petrovas et al., 2006; Zander et al., 2019), adoptive transfer experiments suggested that T_{Exh} cells had lower survival rates than T_E cells. Indeed, 1 week after acute LCMV infection of naive recipients that had received sorted populations, the recovery rate of cells initially in a T_{Exh} state was lower than the recovery rate of T_E or T_I cells. Corroborating previous results, T_M cells had the best expansion and gave rise to all subsets (Im et al., 2016; Utzschneider et al., 2016b; Jeannet et al., 2010). Moreover, all four P14 subsets harvested 21 dpi showed plasticity when transferred into naive hosts, followed by LCMV infection, but not when transferred into chronically infected mice, suggesting the lack of plasticity observed in persistently infected mice 21 dpi is probably not cell intrinsic and likely due to differences in antigen load and/or (anti)-inflammatory environments at different stages of chronic infection.

This work presents relevant insights into the phenotypic landscape of P14 cells constantly stimulated with cognate antigen, highlighting their phenotypic diversity in chronic LCMV infection. These findings are relevant in the context of T cell exhaustion in chronic infections, as well as cancer, showing that the phenotype of virus-specific CD8 T cells is shaped by the microenvironment and is largely plastic.

STAR★METHODS

Detailed methods are provided in the online version of this paper and include the following:

- KEY RESOURCES TABLE
- RESOURCE AVAILABILITY
  - Lead Contact
  - Materials Availability
  - Data and Code Availability
- EXPERIMENTAL MODEL AND SUBJECT DETAILS
- METHOD DETAILS
  - Virus
  - Infections
  - Cell isolation from tissues
  - scRNaseq analysis
  - Adoptive transfer experiments
  - P14 restimulation
  - Flow cytometry analysis
  - Determination of viral loads
  - Heatmaps and PCA analysis
  - Cell densities and high-dimensional clustering
  - *In vivo* labeling
  - Batch correction
- QUANTIFICATION AND STATISTICAL ANALYSIS

SUPPLEMENTAL INFORMATION

Supplemental Information can be found online at https://doi.org/10.1016/j.celrep.2020.108078.

ACKNOWLEDGMENTS

We are grateful to the members of the Claassen, Oxenius, and Joller (University of Zurich) groups for helpful discussions and feedback. This work was supported by the ETH Zurich (grant ETH-39 14-2 to M.C. and A.O.).

AUTHOR CONTRIBUTIONS

Conceptualization, I.S., M.C., A.O.; Methodology, I.S., D.C., M.B., N.O., F.W., I.S., S.P.M.W.; Investigation, I.S., U.S., M.C., A.O.; Writing, I.S., M.C., A.O.; Funding Acquisition, Resources, and Supervision, M.C. and A.O.

DECLARATION OF INTERESTS

The authors declare no competing interests.

Received: June 25, 2019
Revised: January 31, 2020
Accepted: August 5, 2020
Published: August 25, 2020

REFERENCES

Abel, S., Hundhausen, C., Mentlein, R., Schulte, A., Berkhout, T.A., Broadway, N., Hartmann, D., Sedlacek, R., Dietrich, S., Muetze, B., et al. (2004). The transmembrane CXC-chemokine ligand 16 is induced by IFN-gamma and TNF-alpha and shed by the activity of the disintegrin-like metalloproteinase ADAM10. J. Immunol. *172*, 6362–6372.

Agnellini, P., Wolint, P., Rehr, M., Cahenzli, J., Karrer, U., and Oxenius, A. (2007). Impaired NFAT nuclear translocation results in split exhaustion of virus-specific CD8+ T cell functions during chronic viral infection. Proc. Natl. Acad. Sci. USA *104*, 4565–4570.

Alfei, F., Kanev, K., Hofmann, M., Wu, M., Ghoneim, H.E., Roelli, P., Utzschneider, D.T., von Hoesslin, M., Cullen, J.G., Fan, Y., et al. (2019). TOX reinforces the phenotype and longevity of exhausted T cells in chronic viral infection. Nature *571*, 265–269.

Althage, A., Odermatt, B., Moskophidis, D., Kündig, T., Hoffman-Rohrer, U., Hengartner, H., and Zinkernagel, R.M. (1992). Immunosuppression by lymphocytic choriomeningitis virus infection: competent effector T and B cells but impaired antigen presentation. Eur. J. Immunol. *22*, 1803–1812.

Andersson, E.C., Christensen, J.P., Scheynius, A., Marker, O., and Thomsen, A.R. (1995). Lymphocytic choriomeningitis virus infection is associated with long-standing perturbation of LFA-1 expression on CD8+ T cells. Scand. J. Immunol. *42*, 110–118.

Angelosanto, J.M., Blackburn, S.D., Crawford, A., and Wherry, E.J. (2012). Progressive loss of memory T cell potential and commitment to exhaustion during chronic viral infection. J. Virol. *86*, 8161–8170.

Argilaguet, J., Pedragosa, M., Esteve-Codina, A., Riera, G., Vidal, E., Peligero-Cruz, C., Casella, V., Andreu, D., Kaisho, T., Bocharov, G., et al. (2019). Systems analysis reveals complex biological processes during virus infection fate decisions. Genome Res. *29*, 907–919.

Ashburner, M., Ball, C.A., Blake, J.A., Botstein, D., Butler, H., Cherry, J.M., Davis, A.P., Dolinski, K., Dwight, S.S., Eppig, J.T., et al.; The Gene Ontology Consortium (2000). Gene ontology: tool for the unification of biology. Nat. Genet. *25*, 25–29.

Ashouri, J.F., and Weiss, A. (2017). Endogenous Nur77 Is a Specific Indicator of Antigen Receptor Signaling in Human T and B Cells. J. Immunol. *198*, 657–668.

Barber, D.L., Wherry, E.J., Masopust, D., Zhu, B., Allison, J.P., Sharpe, A.H., Freeman, G.J., and Ahmed, R. (2006). Restoring function in exhausted CD8 T cells during chronic viral infection. Nature *439*, 682–687.

Battegay, M., Cooper, S., Althage, A., Bänziger, J., Hengartner, H., and Zinkernagel, R.M. (1991). Quantification of lymphocytic choriomeningitis virus with an immunological focus assay in 24- or 96-well plates. J. Virol. Methods *33*, 191–198.

Baumann, N.S., Torti, N., Welten, S.P.M., Barnstorf, I., Borsa, M., Pallmer, K., Oduro, J.D., Cicin-Sain, L., Ikuta, K., Ludewig, B., and Oxenius, A. (2018). Tissue maintenance of CMV-specific inflationary memory T cells by IL-15. PLoS Pathog. *14*, e1006993.

Beltra, J.C., Bourbonnais, S., Bédard, N., Charpentier, T., Boulangé, M., Michaud, E., Boufaied, I., Bruneau, J., Shoukry, N.H., Lamarre, A., and Decaluwe, H. (2016). IL2Rβ-dependent signals drive terminal exhaustion and suppress memory development during chronic viral infection. Proc. Natl. Acad. Sci. USA *113*, E5444–E5453.

Beltra, J.C., Manne, S., Abdel-Hakeem, M.S., Kurachi, M., Giles, J.R., Chen, Z., Casella, V., Ngiow, S.F., Khan, O., Huang, Y.J., et al. (2020). Developmental Relationships of Four Exhausted CD8+ T Cell Subsets Reveals Underlying Transcriptional and Epigenetic Landscape Control Mechanisms. Immunity *52*, 825–841.e8.

Benjamini, Y., and Hochberg, Y. (1995). Controlling the False Discovery Rate - a Practical and Powerful Approach to Multiple Testing. J. R. Stat. Soc. Series B Stat. Methodol. *57*, 289–300.

Berg, E.L., Robinson, M.K., Warnock, R.A., and Butcher, E.C. (1991). The human peripheral lymph node vascular addressin is a ligand for LECAM-1, the peripheral lymph node homing receptor. J. Cell Biol. *114*, 343–349.

Bertram, E.M., Tafuri, A., Shahinian, A., Chan, V.S.F., Hunziker, L., Recher, M., Ohashi, P.S., Mak, T.W., and Watts, T.H. (2002). Role of ICOS versus CD28 in antiviral immunity. Eur. J. Immunol. *32*, 3376–3385.

Blackburn, S.D., Shin, H., Haining, W.N., Zou, T., Workman, C.J., Polley, A., Betts, M.R., Freeman, G.J., Vignali, D.A., and Wherry, E.J. (2009). Coregulation of CD8+ T cell exhaustion by multiple inhibitory receptors during chronic viral infection. Nat. Immunol. *10*, 29–37.

Blackburn, S.D., Crawford, A., Shin, H., Polley, A., Freeman, G.J., and Wherry, E.J. (2010). Tissue-specific differences in PD-1 and PD-L1 expression during chronic viral infection: implications for CD8 T-cell exhaustion. J. Virol. *84*, 2078–2089.

Borsa, M., Barnstorf, I., Baumann, N.S., Pallmer, K., Yermanos, A., Gräbnitz, F., Barandun, N., Hausmann, A., Sandu, I., Barral, Y., and Oxenius, A. (2019). Modulation of asymmetric cell division as a mechanism to boost $CD8^+$ T cell memory. Sci. Immunol. *4*, eaav1730.

Bucks, C.M., Norton, J.A., Boesteanu, A.C., Mueller, Y.M., and Katsikis, P.D. (2009). Chronic antigen stimulation alone is sufficient to drive CD8+ T cell exhaustion. J. Immunol. *182*, 6697–6708.

Buettner, F., Pratanwanich, N., McCarthy, D.J., Marioni, J.C., and Stegle, O. (2017). f-scLVM: scalable and versatile factor analysis for single-cell RNA-seq. Genome Biol. *18*, 212.

Butler, A., Hoffman, P., Smibert, P., Papalexi, E., and Satija, R. (2018). Integrating single-cell transcriptomic data across different conditions, technologies, and species. Nat. Biotechnol. *36*, 411–420.

Chaix, J., Nish, S.A., Lin, W.H., Rothman, N.J., Ding, L., Wherry, E.J., and Reiner, S.L. (2014). Cutting edge: CXCR4 is critical for CD8+ memory T cell homeostatic self-renewal but not rechallenge self-renewal. J. Immunol. *193*, 1013–1016.

Chamoto, K., Chowdhury, P.S., Kumar, A., Sonomura, K., Matsuda, F., Fagarasan, S., and Honjo, T. (2017). Mitochondrial activation chemicals synergize with surface receptor PD-1 blockade for T cell-dependent antitumor activity. Proc. Natl. Acad. Sci. USA *114*, E761–E770.

Chen, Z., Ji, Z., Ngiow, S.F., Manne, S., Cai, Z., Huang, A.C., Johnson, J., Staupe, R.P., Bengsch, B., Xu, C., et al. (2019). TCF-1-Centered Transcriptional Network Drives an Effector versus Exhausted CD8 T Cell-Fate Decision. Immunity *51*, 840–855.e5.

Christensen, J.P., Andersson, E.C., Scheynius, A., Marker, O., and Thomsen, A.R. (1995). Alpha 4 integrin directs virus-activated CD8+ T cells to sites of infection. J. Immunol. *154*, 5293–5301.

Christensen, J.E., Andreasen, S.O., Christensen, J.P., and Thomsen, A.R. (2001). CD11b expression as a marker to distinguish between recently activated effector CD8(+) T cells and memory cells. Int. Immunol. *13*, 593–600.

Ciurea, A., Klenerman, P., Hunziker, L., Horvath, E., Odermatt, B., Ochsenbein, A.F., Hengartner, H., and Zinkernagel, R.M. (1999). Persistence of lymphocytic choriomeningitis virus at very low levels in immune mice. Proc. Natl. Acad. Sci. USA *96*, 11964–11969.

Culhane, A.C., Thioulouse, J., Perrière, G., and Higgins, D.G. (2005). MADE4: an R package for multivariate analysis of gene expression data. Bioinformatics *21*, 2789–2790.

Doering, T.A., Crawford, A., Angelosanto, J.M., Paley, M.A., Ziegler, C.G., and Wherry, E.J. (2012). Network analysis reveals centrally connected genes and pathways involved in CD8+ T cell exhaustion versus memory. Immunity *37*, 1130–1144.

Dohi, T., Okada, K., Xia, F., Wilford, C.E., Samuel, T., Welsh, K., Marusawa, H., Zou, H., Armstrong, R., Matsuzawa, S., et al. (2004). An IAP-IAP complex inhibits apoptosis. J. Biol. Chem. *279*, 34087–34090.

Dominguez, C.X., Amezquita, R.A., Guan, T., Marshall, H.D., Joshi, N.S., Kleinstein, S.H., and Kaech, S.M. (2015). The transcription factors ZEB2 and T-bet cooperate to program cytotoxic T cell terminal differentiation in response to LCMV viral infection. J. Exp. Med. *212*, 2041–2056.

Ebnet, K., Chluba-de Tapia, J., Hurtenbach, U., Kramer, M.D., and Simon, M.M. (1991). In vivo primed mouse T cells selectively express T cell-specific serine proteinase-1 and the proteinase-like molecules granzyme B and C. Int. Immunol. *3*, 9–19.

Erickson, J.J., Lu, P., Wen, S., Hastings, A.K., Gilchuk, P., Joyce, S., Shyr, Y., and Williams, J.V. (2015). Acute Viral Respiratory Infection Rapidly Induces a CD8+ T Cell Exhaustion-like Phenotype. J. Immunol. *195*, 4319–4330.

Farber, J.M. (1997). Mig and IP-10: CXC chemokines that target lymphocytes. J. Leukoc. Biol. *61*, 246–257.

Fong, A.M., Robinson, L.A., Steeber, D.A., Tedder, T.F., Yoshie, O., Imai, T., and Patel, D.D. (1998). Fractalkine and CX3CR1 mediate a novel mechanism of leukocyte capture, firm adhesion, and activation under physiologic flow. J. Exp. Med. *188*, 1413–1419.

Frebel, H., and Oxenius, A. (2013). The risks of targeting co-inhibitory pathways to modulate pathogen-directed T cell responses. Trends Immunol. *34*, 193–199.

Frebel, H., Nindl, V., Schuepbach, R.A., Braunschweiler, T., Richter, K., Vogel, J., Wagner, C.A., Loffing-Cueni, D., Kurrer, M., Ludewig, B., and Oxenius, A. (2012). Programmed death 1 protects from fatal circulatory failure during systemic virus infection of mice. J. Exp. Med. *209*, 2485–2499.

Fröhlich, A., Kisielow, J., Schmitz, I., Freigang, S., Shamshiev, A.T., Weber, J., Marsland, B.J., Oxenius, A., and Kopf, M. (2009). IL-21R on T cells is critical for sustained functionality and control of chronic viral infection. Science *324*, 1576–1580.

Fuller, M.J., Khanolkar, A., Tebo, A.E., and Zajac, A.J. (2004). Maintenance, loss, and resurgence of T cell responses during acute, protracted, and chronic viral infections. J. Immunol. *172*, 4204–4214.

Garcia, V., Richter, K., Graw, F., Oxenius, A., and Regoes, R.R. (2015). Estimating the In Vivo Killing Efficacy of Cytotoxic T Lymphocytes across Different Peptide-MHC Complex Densities. PLoS Comput. Biol. *11*, e1004178.

The Gene Ontology Consortium (2019). The Gene Ontology Resource: 20 years and still GOing strong. Nucleic Acids Res. *47* (*D1*), D330–D338.

Gerdes, J., Lemke, H., Baisch, H., Wacker, H.H., Schwab, U., and Stein, H. (1984). Cell cycle analysis of a cell proliferation-associated human nuclear antigen defined by the monoclonal antibody Ki-67. J. Immunol. *133*, 1710–1715.

Gerlach, C., Moseman, E.A., Loughhead, S.M., Alvarez, D., Zwijnenburg, A.J., Waanders, L., Garg, R., de la Torre, J.C., and von Andrian, U.H. (2016). The Chemokine Receptor CX3CR1 Defines Three Antigen-Experienced CD8 T Cell Subsets with Distinct Roles in Immune Surveillance and Homeostasis. Immunity *45*, 1270–1284.

Godec, J., Tan, Y., Liberzon, A., Tamayo, P., Bhattacharya, S., Butte, A.J., Mesirov, J.P., and Haining, W.N. (2016). Compendium of Immune Signatures Identifies Conserved and Species-Specific Biology in Response to Inflammation. Immunity *44*, 194–206.

Graw, F., Richter, K., Oxenius, A., and Regoes, R.R. (2011). Comparison of cytotoxic T lymphocyte efficacy in acute and persistent lymphocytic choriomeningitis virus infection. Proc. Biol. Sci. *278*, 3395–3402.

Groh, V., Rhinehart, R., Randolph-Habecker, J., Topp, M.S., Riddell, S.R., and Spies, T. (2001). Costimulation of CD8alphabeta T cells by NKG2D via engagement by MIC induced on virus-infected cells. Nat. Immunol. *2*, 255–260.

Gunn, M.D., Tangemann, K., Tam, C., Cyster, J.G., Rosen, S.D., and Williams, L.T. (1998). A chemokine expressed in lymphoid high endothelial venules promotes the adhesion and chemotaxis of naive T lymphocytes. Proc. Natl. Acad. Sci. USA *95*, 258–263.

Gupta, P.K., Godec, J., Wolski, D., Adland, E., Yates, K., Pauken, K.E., Cosgrove, C., Ledderose, C., Junger, W.G., Robson, S.C., et al. (2015). CD39 Expression Identifies Terminally Exhausted CD8+ T Cells. PLoS Pathog. *11*, e1005177.

Hu, J.K., Kagari, T., Clingan, J.M., and Matloubian, M. (2011). Expression of chemokine receptor CXCR3 on T cells affects the balance between effector and memory CD8 T-cell generation. Proc. Natl. Acad. Sci. USA *108*, E118–E127.

Hudson, W.H., Gensheimer, J., Hashimoto, M., Wieland, A., Valanparambil, R.M., Li, P., Lin, J.X., Konieczny, B.T., Im, S.J., Freeman, G.J., et al. (2019). Proliferating Transitory T Cells with an Effector-like Transcriptional Signature Emerge from PD-1(+) Stem-like CD8(+) T Cells during Chronic Infection. Immunity *51*, 1043–1058.e4.

Im, S.J., Hashimoto, M., Gerner, M.Y., Lee, J., Kissick, H.T., Burger, M.C., Shan, Q., Hale, J.S., Lee, J., Nasti, T.H., et al. (2016). Defining CD8+ T cells that provide the proliferative burst after PD-1 therapy. Nature *537*, 417–421.

Ingram, J.T., Yi, J.S., and Zajac, A.J. (2011). Exhausted CD8 T cells downregulate the IL-18 receptor and become unresponsive to inflammatory cytokines and bacterial co-infections. PLoS Pathog. *7*, e1002273.

Jeannet, G., Boudousquié, C., Gardiol, N., Kang, J., Huelsken, J., and Held, W. (2010). Essential role of the Wnt pathway effector Tcf-1 for the establishment of functional CD8 T cell memory. Proc. Natl. Acad. Sci. USA *107*, 9777–9782.

Khan, O., Giles, J.R., McDonald, S., Manne, S., Ngiow, S.F., Patel, K.P., Werner, M.T., Huang, A.C., Alexander, K.A., Wu, J.E., et al. (2019). TOX transcriptionally and epigenetically programs $CD8^+$ T cell exhaustion. Nature *571*, 211–218.

Knell, J., Best, J.A., Lind, N.A., Yang, E., D'Cruz, L.M., and Goldrath, A.W. (2013). Id2 influences differentiation of killer cell lectin-like receptor G1(hi) short-lived CD8+ effector T cells. J. Immunol. *190*, 1501–1509.

Korotkevich, G., Sukhov, V., and Sergushichev, A. (2019). Fast gene set enrichment analysis. bioRxiv. https://doi.org/10.1101/060012.

Korsunsky, I., Millard, N., Fan, J., Slowikowski, K., Zhang, F., Wei, K., Baglaenko, Y., Brenner, M., Loh, P.R., and Raychaudhuri, S. (2019). Fast, sensitive and accurate integration of single-cell data with Harmony. Nat. Methods *16*, 1289–1296.

Landt, S.G., Marinov, G.K., Kundaje, A., Kheradpour, P., Pauli, F., Batzoglou, S., Bernstein, B.E., Bickel, P., Brown, J.B., Cayting, P., et al. (2012). ChIP-seq guidelines and practices of the ENCODE and modENCODE consortia. Genome Res. *22*, 1813–1831.

Lee, D.M., Staats, H.F., Sundy, J.S., Patel, D.D., Sempowski, G.D., Scearce, R.M., Jones, D.M., and Haynes, B.F. (1998). Immunologic characterization of CD7-deficient mice. J. Immunol. *160*, 5749–5756.

Leong, Y.A., Chen, Y., Ong, H.S., Wu, D., Man, K., Deleage, C., Minnich, M., Meckiff, B.J., Wei, Y., Hou, Z., et al. (2016). CXCR5(+) follicular cytotoxic T cells control viral infection in B cell follicles. Nat. Immunol. *17*, 1187–1196.

Li, Y., and Benezra, R. (1996). Identification of a human mitotic checkpoint gene: hsMAD2. Science *274*, 246–248.

Lin, Y., Roberts, T.J., Sriram, V., Cho, S., and Brutkiewicz, R.R. (2003). Myeloid marker expression on antiviral CD8+ T cells following an acute virus infection. Eur. J. Immunol. *33*, 2736–2743.

Maaten, L.V.D., and Hinton, G. (2008). Visualizing data using t-SNE. J. Mach. Learn. Res. *9*, 2579–2605.

Mackerness, K.J., Cox, M.A., Lilly, L.M., Weaver, C.T., Harrington, L.E., and Zajac, A.J. (2010). Pronounced virus-dependent activation drives exhaustion but sustains IFN-γ transcript levels. J. Immunol. *185*, 3643–3651.

Mann, M., and Jensen, O.N. (2003). Proteomic analysis of post-translational modifications. Nat. Biotechnol. *21*, 255–261.

Matloubian, M., David, A., Engel, S., Ryan, J.E., and Cyster, J.G. (2000). A transmembrane CXC chemokine is a ligand for HIV-coreceptor Bonzo. Nat. Immunol. *1*, 298–304.

Miller, B.C., Sen, D.R., Al Abosy, R., Bi, K., Virkud, Y.V., LaFleur, M.W., Yates, K.B., Lako, A., Felt, K., Naik, G.S., et al. (2019). Subsets of exhausted $CD8^+$ T cells differentially mediate tumor control and respond to checkpoint blockade. Nat. Immunol. *20*, 326–336.

Mims, C.A., and Wainwright, S. (1968). The immunodepressive action of lymphocytic choriomeningitis virus in mice. J. Immunol. *101*, 717–724.

Moran, A.E., Holzapfel, K.L., Xing, Y., Cunningham, N.R., Maltzman, J.S., Punt, J., and Hogquist, K.A. (2011). T cell receptor signal strength in Treg and iNKT cell development demonstrated by a novel fluorescent reporter mouse. J. Exp. Med. *208*, 1279–1289.

Mueller, S.N., and Ahmed, R. (2009). High antigen levels are the cause of T cell exhaustion during chronic viral infection. Proc. Natl. Acad. Sci. USA *106*, 8623–8628.

Mundt, A.K.A.F. (2019). factoextra: Extract and Visualize the Results of Multivariate Data Analyses. https://rpkgs.datanovia.com/factoextra/index.html.

Odermatt, B., Eppler, M., Leist, T.P., Hengartner, H., and Zinkernagel, R.M. (1991). Virus-triggered acquired immunodeficiency by cytotoxic T-cell-dependent destruction of antigen-presenting cells and lymph follicle structure. Proc. Natl. Acad. Sci. USA *88*, 8252–8256.

Paillard, F., Sterkers, G., and Vaquero, C. (1990). Transcriptional and post-transcriptional regulation of TcR, CD4 and CD8 gene expression during activation of normal human T lymphocytes. EMBO J. *9*, 1867–1872.

Paley, M.A., Gordon, S.M., Bikoff, E.K., Robertson, E.J., Wherry, E.J., and Reiner, S.L. (2013). Technical Advance: Fluorescent reporter reveals insights into eomesodermin biology in cytotoxic lymphocytes. J. Leukoc. Biol. *93*, 307–315.

Pan, Y., Lloyd, C., Zhou, H., Dolich, S., Deeds, J., Gonzalo, J.A., Vath, J., Gosselin, M., Ma, J., Dussault, B., et al. (1997). Neurotactin, a membrane-anchored chemokine upregulated in brain inflammation. Nature *387*, 611–617.

Peperzak, V., Veraar, E.A., Xiao, Y., Babala, N., Thiadens, K., Brugmans, M., and Borst, J. (2013). CD8+ T cells produce the chemokine CXCL10 in response to CD27/CD70 costimulation to promote generation of the CD8+ effector T cell pool. J. Immunol. *191*, 3025–3036.

Petrovas, C., Casazza, J.P., Brenchley, J.M., Price, D.A., Gostick, E., Adams, W.C., Precopio, M.L., Schacker, T., Roederer, M., Douek, D.C., and Koup, R.A. (2006). PD-1 is a regulator of virus-specific CD8+ T cell survival in HIV infection. J. Exp. Med. *203*, 2281–2292.

Pircher, H., Moskophidis, D., Rohrer, U., Bürki, K., Hengartner, H., and Zinkernagel, R.M. (1990). Viral escape by selection of cytotoxic T cell-resistant virus variants in vivo. Nature *346*, 629–633.

R Development Core Team (2019). R: A language and environment for statistical computing (R Foundation for Statistical Computing).

Richter, K., Agnellini, P., and Oxenius, A. (2010). On the role of the inhibitory receptor LAG-3 in acute and chronic LCMV infection. Int. Immunol. *22*, 13–23.

Ritchie, M.E., Phipson, B., Wu, D., Hu, Y., Law, C.W., Shi, W., and Smyth, G.K. (2015). limma powers differential expression analyses for RNA-sequencing and microarray studies. Nucleic Acids Res. *43*, e47.

Sato, M., Hata, N., Asagiri, M., Nakaya, T., Taniguchi, T., and Tanaka, N. (1998). Positive feedback regulation of type I IFN genes by the IFN-inducible transcription factor IRF-7. FEBS Lett. *441*, 106–110.

Sato, N., Patel, H.J., Waldmann, T.A., and Tagaya, Y. (2007). The IL-15/IL-15Ralpha on cell surfaces enables sustained IL-15 activity and contributes to the long survival of CD8 memory T cells. Proc. Natl. Acad. Sci. USA *104*, 588–593.

Schmitz, I., Schneider, C., Fröhlich, A., Frebel, H., Christ, D., Leonard, W.J., Sparwasser, T., Oxenius, A., Freigang, S., and Kopf, M. (2013). IL-21 restricts virus-driven Treg cell expansion in chronic LCMV infection. PLoS Pathog. *9*, e1003362.

Scott-Browne, J.P., López-Moyado, I.F., Trifari, S., Wong, V., Chavez, L., Rao, A., and Pereira, R.M. (2016). Dynamic Changes in Chromatin Accessibility Occur in CD8$^+$ T Cells Responding to Viral Infection. Immunity *45*, 1327–1340.

Sen, D.R., Kaminski, J., Barnitz, R.A., Kurachi, M., Gerdemann, U., Yates, K.B., Tsao, H.W., Godec, J., LaFleur, M.W., Brown, F.D., et al. (2016). The epigenetic landscape of T cell exhaustion. Science *354*, 1165–1169.

Seo, H., Chen, J., González-Avalos, E., Samaniego-Castruita, D., Das, A., Wang, Y.H., López-Moyado, I.F., Georges, R.O., Zhang, W., Onodera, A., et al. (2019). TOX and TOX2 transcription factors cooperate with NR4A transcription factors to impose CD8$^+$ T cell exhaustion. Proc. Natl. Acad. Sci. USA *116*, 12410–12415.

Shin, H., Blackburn, S.D., Blattman, J.N., and Wherry, E.J. (2007). Viral antigen and extensive division maintain virus-specific CD8 T cells during chronic infection. J. Exp. Med. *204*, 941–949.

Skon, C.N., Lee, J.Y., Anderson, K.G., Masopust, D., Hogquist, K.A., and Jameson, S.C. (2013). Transcriptional downregulation of S1pr1 is required for the establishment of resident memory CD8+ T cells. Nat. Immunol. *14*, 1285–1293.

Subramanian, A., Tamayo, P., Mootha, V.K., Mukherjee, S., Ebert, B.L., Gillette, M.A., Paulovich, A., Pomeroy, S.L., Golub, T.R., Lander, E.S., and Mesirov, J.P. (2005). Gene set enrichment analysis: a knowledge-based approach for interpreting genome-wide expression profiles. Proc. Natl. Acad. Sci. USA *102*, 15545–15550.

Svensson, V., Natarajan, K.N., Ly, L.H., Miragaia, R.J., Labalette, C., Macaulay, I.C., Cvejic, A., and Teichmann, S.A. (2017). Power analysis of single-cell RNA-sequencing experiments. Nat. Methods *14*, 381–387.

Szklarczyk, D., Gable, A.L., Lyon, D., Junge, A., Wyder, S., Huerta-Cepas, J., Simonovic, M., Doncheva, N.T., Morris, J.H., Bork, P., et al. (2019). STRING v11: protein-protein association networks with increased coverage, supporting functional discovery in genome-wide experimental datasets. Nucleic Acids Res. *47* (*D1*), D607–D613.

Thom, J.T., Weber, T.C., Walton, S.M., Torti, N., and Oxenius, A. (2015). The Salivary Gland Acts as a Sink for Tissue-Resident Memory CD8(+) T Cells, Facilitating Protection from Local Cytomegalovirus Infection. Cell Rep. *13*, 1125–1136.

Utzschneider, D.T., Alfei, F., Roelli, P., Barras, D., Chennupati, V., Darbre, S., Delorenzi, M., Pinschewer, D.D., and Zehn, D. (2016a). High antigen levels induce an exhausted phenotype in a chronic infection without impairing T cell expansion and survival. J. Exp. Med. *213*, 1819–1834.

Utzschneider, D.T., Charmoy, M., Chennupati, V., Pousse, L., Ferreira, D.P., Calderon-Copete, S., Danilo, M., Alfei, F., Hofmann, M., Wieland, D., et al. (2016b). T Cell Factor 1-Expressing Memory-like CD8(+) T Cells Sustain the Immune Response to Chronic Viral Infections. Immunity *45*, 415–427.

Utzschneider, D.T., Delpoux, A., Wieland, D., Huang, X., Lai, C.Y., Hofmann, M., Thimme, R., and Hedrick, S.M. (2018). Active Maintenance of T Cell Memory in Acute and Chronic Viral Infection Depends on Continuous Expression of FOXO1. Cell Rep. *22*, 3454–3467.

Van Gassen, S., Callebaut, B., Van Helden, M.J., Lambrecht, B.N., Demeester, P., Dhaene, T., and Saeys, Y. (2015). FlowSOM: Using self-organizing maps for visualization and interpretation of cytometry data. Cytometry A *87*, 636–645.

Walunas, T.L., Bruce, D.S., Dustin, L., Loh, D.Y., and Bluestone, J.A. (1995). Ly-6C is a marker of memory CD8+ T cells. J. Immunol. *155*, 1873–1883.

Westgaard, I.H., Dissen, E., Torgersen, K.M., Lazetic, S., Lanier, L.L., Phillips, J.H., and Fossum, S. (2003). The lectin-like receptor KLRE1 inhibits natural killer cell cytotoxicity. J. Exp. Med. *197*, 1551–1561.

Wherry, E.J., Blattman, J.N., Murali-Krishna, K., van der Most, R., and Ahmed, R. (2003). Viral persistence alters CD8 T-cell immunodominance and tissue distribution and results in distinct stages of functional impairment. J. Virol. *77*, 4911–4927.

Wherry, E.J., Ha, S.J., Kaech, S.M., Haining, W.N., Sarkar, S., Kalia, V., Subramaniam, S., Blattman, J.N., Barber, D.L., and Ahmed, R. (2007). Molecular signature of CD8+ T cell exhaustion during chronic viral infection. Immunity *27*, 670–684.

Wickham, H. (2016). ggplot2: Elegant Graphics for Data Analysis. https://ggplot2.tidyverse.org/index.html.

Wilcoxon, F. (1945). Individual Comparisons by Ranking Methods. Biometics Bull. *1*, 80–83.

Xin, G., Schauder, D.M., Lainez, B., Weinstein, J.S., Dai, Z., Chen, Y., Esplugues, E., Wen, R., Wang, D., Parish, I.A., et al. (2015). A Critical Role of IL-21-Induced BATF in Sustaining CD8-T-Cell-Mediated Chronic Viral Control. Cell Rep. *13*, 1118–1124.

Yamazaki, C., Sugiyama, M., Ohta, T., Hemmi, H., Hamada, E., Sasaki, I., Fukuda, Y., Yano, T., Nobuoka, M., Hirashima, T., et al. (2013). Critical roles of a dendritic cell subset expressing a chemokine receptor, XCR1. J. Immunol. *190*, 6071–6082.

Yao, C., Sun, H.W., Lacey, N.E., Ji, Y., Moseman, E.A., Shih, H.Y., Heuston, E.F., Kirby, M., Anderson, S., Cheng, J., et al. (2019). Single-cell RNA-seq reveals TOX as a key regulator of CD8$^+$ T cell persistence in chronic infection. Nat. Immunol. *20*, 890–901.

Yi, J.S., Du, M., and Zajac, A.J. (2009). A vital role for interleukin-21 in the control of a chronic viral infection. Science *324*, 1572–1576.

Yu, G., Wang, L.-G., Han, Y., and He, Q.-Y. (2012). clusterProfiler: an R package for comparing biological themes among gene clusters. OMICS *16*, 284–287.

Zander, R., Schauder, D., Xin, G., Nguyen, C., Wu, X., Zajac, A., and Cui, W. (2019). CD4(+) T Cell Help Is Required for the Formation of a Cytolytic CD8(+) T Cell Subset that Protects against Chronic Infection and Cancer. Immunity *51*, 1028–1042.e4.

Zheng, G.X., Terry, J.M., Belgrader, P., Ryvkin, P., Bent, Z.W., Wilson, R., Ziraldo, S.B., Wheeler, T.D., McDermott, G.P., Zhu, J., et al. (2017). Massively parallel digital transcriptional profiling of single cells. Nat. Commun. *8*, 14049.

STAR★METHODS

KEY RESOURCES TABLE

REAGENT or RESOURCE	SOURCE	IDENTIFIER
Antibodies		
B220 (biotin, RA3-6B2)	Biolegend	Cat#103204; RRID:AB_312989
CD107a (PE, 1D4R)	Biolegend	Cat# 103043; RRID: AB_2134487
CD28 (37.51)	Biolegend	Cat#102116; RRID: AB_11147170
CD39 (AF647, Duha59)	Biolegend	Cat#143807; RRID: AB_2563977
CD3ξ (145-2C11)	Biolegend	Cat#100340, RRID: AB_11149115
CD4 (biotin, GK1.5)	Biolegend	Cat#100404; RRID: AB_312689
CD44 (BV510, IM7)	Biolegend	Cat#102116; RRID: AB_2561391
CD45.1 (APC, A20)	Biolegend	Cat# 110714; RRID: AB_313503
CD45.1 (BV711, A20)	Biolegend	Cat#110739; RRID: AB_2562605
CD45.1 (Pacific Blue, A20)	Biolegend	Cat# 110722; RRID: AB_492866
CD5 (PE-Cy7, 53-7.3)	Biolegend	Cat#100622; RRID: AB_2562773
CD8 (APC-Cy7, 53-6.7)	Biolegend	Cat#102116; RRID: AB_11147170
CD8 (BUV395, 53-6.7)	Biolegend	Cat#102116; RRID: AB_312753
CD8 (BV711, 53-6.7)	Biolegend	Cat# 100714; RRID: AB_11147170
CD8 (PerCP, 53-6.7)	Biolegend	Cat# 100732; RRID: AB_893423
CD8b.2 (PE, 53-5.8)	BD Biosciences	Cat#553041; RRID: AB_394577
CX3CR1 (APC, SA011F11)	Biolegend	Cat#102116; RRID: AB_2564491
CX3CR1 (PerCP-Cy5.5, SA011F11)	Biolegend	Cat#149010; RRID: AB_2566545
CXCR3 (BV421, CXCR3-173)	Biolegend	Cat#102116; RRID: AB_2728154
CXCR6 (PE, SA051D1)	Biolegend	Cat#151103; RRID: AB_11147170
GZMB (PE, GB12)	ThermoFisher	Cat#MHGB04; RRID: AB_10372671
IFNγ (Pacific Blue, XMG1.2)	Biolegend	Cat#505818; RRID: AB_893526
IFNγ (PE, XMG1.2)	ThermoFisher	Cat#12-7311-82; RRID: AB_466193
IgG (peroxidase)	Jackson ImmunoResearch	Cat#:112-035-003, RRID: AB_2338128
Ki67 (Pe-Cy7, SolA15)	ThermoFisher	Cat#25-5698-82; RRID: AB_11220070
LY108 (APC, 330-AJ)	Biolegend	Cat#134609; RRID: AB_11147170
PD-1 (BV605, 29F.1A12)	Biolegend	Cat#135219; RRID: AB_11125371
PD-1 (PE-Cy7, 29F.1A12)	Biolegend	Cat#135215; RRID: AB_10696422
TCF1 (PE, C63D9)	Cell Signaling	Cat#14456S; RRID: AB_2798483
TIM-3 (PE, RMT3-23)	Biolegend	Cat# 119703; RRID: AB_345377
TOX (PE, TXRX10)	ThermoFisher	Cat#12-6502-82; RRID: AB_10855034
VL-4	Generated in-house	N/A
Bacterial and Virus Strains		
LCMV Clone 13	Provided by Dr. Rolf M Zinkernagel (University of Zurich, Switzerland)	(Althage et al., 1992)
Chemicals, Peptides, and Recombinant Proteins		
MEM medium	ThermoFisher	Cat#:31095029
PBS	ThermoFisher	Cat#:14190094
RPMI medium	ThermoFisher	Cat#:11875093
HEPES	ThermoFisher	Cat#:15630056
Non essential amino acids	ThermoFisher	Cat#:11140-035
EDTA	Sigma Aldrich	Cat#:E7889-100ML
Sodium pyruvate	ThermoFisher	Cat#:11360-039
Fetal bovine serum	ThermoFisher	Cat#:10270106

(*Continued on next page*)

Continued

REAGENT or RESOURCE	SOURCE	IDENTIFIER
Penstrep	Sigma	Cat#:P4333
Betamercapthoethanol	ThermoFisher	Cat#:31350-010
Brefeldin A	Biolegend	Cat#:420601
Monensin	Sigma Aldrich	Cat#:M5273-1G
LIVE/DEAD Fixable Near-IR Dye	ThermoFisher	Cat#:L34976
Critical Commercial Assays		
FITC BrdU Flow kit	BD Biosciences	Cat#: 559619
MojoSort™ Streptavidin Nanobeads	Biolegend	Cat#:480016
Chromium Next GEM Single Cell 3′ Library Construction Kit v2	10X Genomics	Cat#:1000157
Fixation Buffer	Biolegend	Cat#:420801
Intracellular Staining Permeabilization Wash Buffer (10X)	Biolegend	Cat#:421002
eBioscience Foxp3 / Transcription Factor Staining Buffer Set	ThermoFisher	Cat#:00-5523-00
Deposited Data		
scRNaseq of exhausted P14 isolated from 6 tissues	This paper	ENA EMBL-EBI: PRJEB36998
Memory-like signature gene list	(Utzschneider et al., 2016b)	N/A
Exhausted signature gene list	(Wherry et al., 2007)	N/A
Effector signature gene list	(Doering et al., 2012)	N/A
C7 immunologic signature gene set collection	(Godec et al., 2016)	N/A
ENCODE ChIP-seq	(Landt et al., 2012)	N/A
GO database	(Ashburner et al., 2000; The Gene Ontology Consortium, 2019)	N/A
Experimental Models: Cell Lines		
BHK-21	Provided by Dr. Rolf M Zinkernagel (University of Zurich, Switzerland)	BHK21 [C13] (ATCC® CCL10)
MC57/G fibroblast	Provided by Dr. Rolf M Zinkernagel (University of Zurich, Switzerland)	MC57G (ATCC® CRL-2295)
VL-4 hybridoma	Provided by Dr. Rolf M Zinkernagel (University of Zurich, Switzerland)	Cat#:006A-EVA92
Experimental Models: Organisms/Strains		
Mouse: C57BL/6	Jaxmice	https://www.jax.org/strain/000664
Mouse: *Tcf7*-GFP reporter mice	Provided by Werner Held (Utzschneider et al., 2016b)	N/A
Mouse: *Nr4a1*-GFP reporter mice	Provided by Roman Spörri (ETH Zurich, Swizterland) (Moran et al., 2011)	https://www.jax.org/strain/016617
Software and Algorithms		
BD FACSDiva Software	BD Biosciences	https://www.bdbiosciences.com/en-us
FlowJo v9, v10	BD Biosciences	https://www.flowjo.com/
Illustrator	Adobe	https://www.adobe.com/products/illustrator.html
CellRanger 2.0.2	(Zheng et al., 2017)	https://support.10xgenomics.com
R	(R Development Core Team, 2019)	https://www.r-project.org/
Seurat v2.0	(Butler et al., 2018)	https://satijalab.org/seurat/
ClusterProfiler	(Yu et al., 2012)	https://guangchuangyu.github.io/software/clusterProfiler/
GSEA	(Subramanian et al., 2005)	https://bioconductor.org/packages/release/bioc/html/GSEABase.html

(*Continued on next page*)

Continued

REAGENT or RESOURCE	SOURCE	IDENTIFIER
fgsea	(Korotkevich et al., 2019)	https://github.com/ctlab/fgsea
slalom	(Buettner et al., 2017)	https://github.com/bioFAM/slalom
FlowSOM	(Van Gassen et al., 2015)	https://github.com/SofieVG/FlowSOM
Limma	(Ritchie et al., 2015)	https://kasperdanielhansen.github.io/genbioconductor/html/limma.html
RtSNE	(Maaten and Hinton, 2008)	https://github.com/jkrijthe/Rtsne
made4	(Culhane et al., 2005)	https://www.bioconductor.org/packages/release/bioc/html/made4.html
ggplot2	(Wickham, 2016)	https://ggplot2.tidyverse.org
stats	(R Development Core Team, 2019)	https://stat.ethz.ch/R-manual/R-devel/library/stats/html/00Index.html
factoextra	(Mundt, 2019)	https://rpkgs.datanovia.com/factoextra/index.html
grDevices	(R Development Core Team, 2019)	https://rdrr.io/r/grDevices/grDevices-package.html
Harmony	(Korsunsky et al., 2019)	https://github.com/immunogenomics/harmony
Prism 8	GraphPad	https://www.graphpad.com/scientific-software/prism/

RESOURCE AVAILABILITY

Lead Contact

Further information and requests for resources and reagents should be directed to and will be fulfilled by the Lead Contact, Annette Oxenius (aoxenius@micro.biol.ethz.ch).

Materials Availability

This study did not generate any new materials.

Data and Code Availability

All software is freely or commercially available and can be found in the Key Resources Table. The accession number for the raw scRNaseq dataset reported in this paper is ENA: PRJEB36998. Further data and materials that supported the findings of this study are available from the corresponding authors upon request.

EXPERIMENTAL MODEL AND SUBJECT DETAILS

Wild-type male C57BL/6J mice (purchased from Janvier Elevage), *Nr4a1* mice expressing a GFP under the control of the NUR77 promoter (Moran et al., 2011), *Tcf7* mice expressing GFP under the control of TCF1 promoter (Utzschneider et al., 2016b), P14 transgenic (CD45.1) mice expressing a TCR specific for LCMV peptide $gp_{33–41}$ (Pircher et al., 1990) were housed and bred under specific pathogen–free conditions at the ETH Phenomics Center Hönggerberg. All mice used in experiments had between 6–16 weeks. P14-*Nr4a1*-GFP and P14-*Tcf7* were generated by crossing P14 mice to *Nr4a1* or *Tcf7* mice. All animal experiments were performed according to the Swiss federal regulations and were approved by the Cantonal Veterinary Office of Zürich (Animal experimentation permissions 147/2014, 115/2017).

METHOD DETAILS

Virus

LCMV clone 13 was propagated in baby hamster kidney 21 (BHK-21) cells at a low multiplicity of infection. 24-72h after infection, supernatant of cultures were harvested. Viral titers were determined as described previously (Battegay et al., 1991).

Infections

10000 transgenic CD45.1$^+$ cells (P14, P14-*Nr4a1* or P14-*Tcf7*) were adoptively transferred into CD45.2$^+$ hosts one day prior LCMV clone 13 infection with 2×10^6 ffu/mouse. For acute infections, 20 ffu LCMV clone 13/mouse were used.

Cell isolation from tissues

Mice were sacrificed with CO_2 and blood was collected from the heart or vena cava into FACS (fluorescence activated cell sorting) buffer. The mice were then perfused with 20 mL of ice-cold PBS, and organs (spleen, BM, lymph nodes, lung, and liver) were isolated. Bone marrow was flushed with 5-10 mL ice-cold PBS. Tissues (lung, liver) were cut into pieces, incubated with digestion cocktail containing 2.4 mg/mL collagenase type II and 0.2 mg/mL DNase in complete RPMI (RPMI-1640 containing 10% fetal bovine serum, 2 mM L-glutamine, 1% penicillin-streptomycin, 1 mM sodium pyruvate, 50 nM betamercapthoethanol, 0.1 mM non-essential (glycine, L-alanine, L-asparagine, L-aspartic acid, L-glutamic acid, L-proline, L-serine) amino acids, 20 mM HEPES) for 30 minutes at 37°C. Cell suspensions were filtered (70 μm) and treated with ammonium-chloride-potassium (ACK) lysis buffer (150 mM NH_4Cl, 10 mM $KHCO_3$, 0,1 nM Na_2EDTA, pH adjusted to 7.3) for 5 min at room temperature. Cell suspension obtained from lungs and liver were enriched for lymphocytes by centrifugation over Percoll density centrifugation (30% (v/v) Percoll in PBS) for 30 minutes at 4°C (500 g). Spleens were depleted of B and CD4 T cells; spleen suspensions were incubated at room temperature with biotinylated α-B220 and α-CD4 for 20 minutes, followed by 5 minute incubation with streptavidin-conjugated magnetic beads (Mojo, Biolegend) and then used StemCell magnet to retain the magnetic beads. For scRNaseq, all tissues (including blood) were incubated with digestion cocktail and treated with ACK lysis buffer. For scRNaseq samples (Figure 1), cell suspension of tissues isolated from three mice were pooled in order to ensure the sample is representative of a population. For cells isolated from lymph nodes, samples from 10 mice were pooled to ensure sufficient P14 cells can be sorted.

scRNaseq analysis

Cell suspensions (see "Cell isolation from tissues") containing P14 cells were next stained with α-CD8a and α-CD45.1 antibodies, and cell viability dye (LiveDead, Thermo Fisher) at 4°C for at least 30 min. P14 cells were then sorted by FACS (ARIA, BD Biosciences) in complete RPMI at 4°C. Sorted P14 cells from different tissues were washed and resuspended in 0.04% BSA. The single cell sequencing was performed at the Functional Genomics Center Zurich. The cell lysis and RNA capture was performed according to the 10XGenomics protocol (Single Cell 3′ v2 chemistry). The cDNA libraries were generated according to the manufacturer's protocol (Illumina) and further sequenced (paired-end) with HiSeq2500 technology (Illumina). The transcripts were mapped with 10Xgenomics CellRanger pipeline (version 2.0.2). The count matrices were analyzed with Seurat package v2.0 (Butler et al., 2018) in R (R Development Core Team, 2019). Briefly, the count matrices were filtered (genes detected in fewer than 10 cells and cells with fewer than 500 transcripts were removed). Outlier cells (based on the correlation between total UMIs and number of detected genes) were also removed. A small cluster of cells displaying a B cell phenotype ($CD3^-CD8^-CD19^+$) was excluded as well. The matrices were normalized (to 10000 transcripts per cell), logged and scaled per gene (mean 0 and variance 1). The contribution of total UMIs counts to the count matrices was regressed out. The resulting matrix was used to select the top 1800 highly expressed and variable genes (based on arbitrary thresholds regarding mean (> 0.1) and gene variance (> 0.2)). These selected genes were used to compute principal components. First 20 principal components were used for graph-based clustering using Louvain modularity (resolution parameter = 0.8). The first 20 principal components were also used for dimensionality reduction (tSNE [Maaten and Hinton, 2008] with perplexity = 50). Next, differential expression analysis (log2 fold change > 0.2) was performed for all detected clusters (using Wilcoxon rank sum test [Wilcoxon, 1945] with multiple test correction [Benjamini and Hochberg, 1995]). Gene set enrichment analysis was done using GSEA package (Subramanian et al., 2005) on the differentially upregulated genes (log2 fold change > 0.5 and adjusted p value < 0.05) in each cluster. Heatmaps were generated in R with made4 package (Culhane et al., 2005). Factor analysis was performed with slalom (Buettner et al., 2017) and C7 immunologic signature collection from MSigDB was used. For GSEA analysis, the ranked gene lists were generated by correlating gene counts with factor values (Spearman correlation). For sample contribution to each cluster, 2500 cells were randomly sampled from each sample. The raw data files have been deposited in the EMBL-EBI database under accession number PRJEB36998.

Adoptive transfer experiments

Organs were harvested from hosts (which received transgenic P14, P14-*Nr4a1*, or P14-*Tcf7* cells one day prior infection) at the indicated time into chronic LCMV infection and processed as described above (see section "Cell isolation from tissues"). For adoptive transfers (Figures 6, 7, S4–S6), between 3 and 12 mice were pooled. Cells were stained and FACS sorted (ARIA, BD Biosciences) based on CD8, CD45.1 and, when indicated, CXCR6, CX3CR1, LY108 or GFP (reporting TCF1 expression). The number of transferred cells was 20 000 (experiments shown in Figures 7B and 7C) and varied between 20 000 and 200 000 for phenotype assessment (Figures 7D and 7E).

P14 restimulation

Restimulations of sorted P14 cells were performed in 96 well flat-bottom antibody-coated plates (α-CD3ξ and α-CD28 at 1 μg/mL) for 6 hours at 37°C in presence of 2 μM monensin, 10 μg/mL brefeldin A, and α-CD107a antibody.

Flow cytometry analysis

Surface stainings were performed at room temperature for 30 minutes in FACS buffer (2% FCS, 1% EDTA in PBS). Intracellular stainings were performed according to the manufacturer's protocol. Data were acquired with LSR II and LSR II Fortessa cytometers (BD Biosciences, Allschwil, Switzerland) and analyzed in FlowJo (BD Biosciences, Allschwil, Switzerland). Bar plots were generated in GraphPad Prism 8 (La Jolla, California, USA).

Determination of viral loads

Viral titers were determined by focus-forming assay using the MC57G fibroblast cell line (Battegay et al., 1991). Blood was collected in FACS buffer, organs were collected in 0.5 mL of MEM medium containing 2% FCS. Tubes were weighted before and after collection of organs. Samples were frozen and stored at −80°C. Organs were homogenized with a tissue lyser. Cell debris was removed by centrifugation at 300 g and supernatant was used for the assay.

Heatmaps and PCA analysis

Heatmaps based on marker medians were generated in R with coolmap (limma package [Ritchie et al., 2015]). Frequencies or marker medians were scaled, then used as input for PCA analysis in R (prcomp function from stats package) and results plotted with factoextra package.

Cell densities and high-dimensional clustering

250 P14 cells were randomly selected for each replicate. Scaled (per gene) marker expression matrix (*Nr4a1*-GFP, CD44, CD8, CD39, TIM-3, PD-1)) was used as input for tSNE calculations (used with default parameters in R implementation, except for the perplexity, which was set to 50). Local 2D scatterplot densities were computed with densCols (grDevices package) function, based on tSNE coordinates (Figure S1). Colors represent relative local densities. FlowSOM was used for high-dimensional clustering of single cells (10x10 grid, n = 15 clusters).

In vivo labeling

In vivo labeling was performed by administering 5 μg of α-CD8a per mouse 3 minutes prior sacrifice as previously described (Thom et al., 2015). Mice were perfused with 20 mL of cold PBS and tissues were processed as described above. For the *in vivo* proliferation assay, 2 mg of BrdU were injected IV 12 hours prior sacrifice. Staining was performed according to the manufacturer's protocol (BD Bioscience).

Batch correction

Harmony was applied on principal components computed after data pre-processing (see "Experimental procedures") without UMI regression. The regression was omitted because the results with respect to the frequency of the memory-like TCF1^{hi} population were closer to expected based on flow cytometry data (data not shown).

QUANTIFICATION AND STATISTICAL ANALYSIS

Unless otherwise mentioned, statistical significance was calculated using Mann-Whitney for comparing two groups. For differential expression analysis (based on scRNaseq data), the non-parametric Wilcoxon rank sum test with Bonferroni correction for multiple comparisons was used. All error bars represent the standard deviation from the mean. All statistical analyses were performed in GraphPad Prism 8 or in R.